Department of Geology and Geophysics

University of Utah

Final Technical Report, No. 1

Title

Kinematics of Basin-Range Intraplate Extension

by

P. K. Eddington, R. B. Smith, and C. Renggli

In Support of

Grant No: NAG 5-164

Project Title: A Study Of Tectonic Activity In The Basin-Range Province And On The San Andreas Fault

Dates: April 15, 1981 to January 31, 1986

Principal Investigator: Robert B. Smith
Professor of Geophysics
Department of Geology and Geophysics
University of Utah
Salt Lake City, Utah 84112-1183

January 1986

submitted to Geol. Soc. London
Symposium volume on Continental
Extensional Tectonics, Nov. 1985

KINEMATICS OF BASIN-RANGE INTRAPLATE EXTENSION

by

Paul K. Eddington and Robert B. Smith
Department of Geology and Geophysics
University of Utah
Salt Lake City, Utah 84112

and

Casper Renggli
Institute for Geophysics
Swiss Federal Institute of Technology
ETH-Honggerberg
CH-8093, Zurich
Switzerland

ABSTRACT

Strain rates assessed from brittle fracture (associated with historic earthquakes) and total brittle-ductile deformation measured from geodetic data have been compared to estimates of paleo-strain from Quaternary geology for the intraplate Great Basin part of the Basin-Range, western United States. These data provide an assessment of the kinematics and mode of lithospheric extension that the western U. S. Cordillera has experienced from the past few million years to the present. Strain and deformation rates were determined by the seismic moment tensor method using historic seismicity and fault plane solutions for sub-regions of homogeneous strain. Contemporary deformation (with maximum deformation rates) in the Great Basin occurs principally along the active seismic zones: 1) the southern Intermountain Seismic Belt (ISB), 4.7 mm/a; 2) along the western boundary, the Sierra Nevada front, 1.6 mm/a (28.0 mm/a if the M8.3 1857 Owen Valley, California is included); and 3) along the west central Nevada seismic belt, 7.5 mm/a. The integrated opening rate across the entire Great Basin is accommodated by E-W extension at 8 to 10 mm/a in the north that diminishes to NW-SE extension of 3.5 mm/a in the south. These results show 8 to 10 mm/a contemporary extension across the entire Great Basin associated with earthquakes that compares to $\leq$9 mm/a determined from tectonic intraplate models (constrained by satellite geodesy) implying that contemporary strain generally released by earthquakes. Zones of maximum lithospheric extension correspond to belts of thin crust, high heat flow, and Quaternary basaltic volcanism, suggesting that these parameters are related through mechanism of extension such as a stress relaxation, allowing bouyant uplift and ascension of magmas.

Contemporary strain and deformation rates have been determined from geodetic measurements yielding maximum deformation at 11.2 mm/a in the Hebgen Lake, Montana portion of the Intermountain Seismic Belt; 3.6 mm/a in the Walker Lane, Nevada area; and 2.5 mm/a in the Owens Valley, California adjacent to the Sierra Nevada front. Paleo-strain and deformation rates principally from Quaternary fault displacement rates gave deformation rates of 7.4 mm/a along the southern ISB. Geodetically determined deformation rates compare well with rates determined from seismic moments. Whereas poorly constrained paleo-strain rates from Quaternary geology are ~10 times smaller than contemporary rates except in parts of central and southern California, Wyoming, parts of Utah, and along the Idaho-Wyoming border.

ACKNOWLEDGMENTS

The research presented here was supported by NASA research grant no. NAG 5-164 on the relationship between the contemporary deformation of the Great Basin and the San Andreas fault. Support for computer time and plotting was from the U.S. Geological Survey grant #14-08-0001-21983. Part of this research was done while one of us (P.K.E.) was a Visiting Graduate Fellow at the Lunar and Planetary Institute, Houston, Texas, which is operated under contract NASW3389.

We particularly acknowledge the earthquake data generously given to us by: R. Cockerham, U.S. Geological Survey, Menlo Park, California; H. Kanamori, California Institute of Technology; A. Ryall, University of Nevada; B. A. Bolt , University of California at Berkeley; S. T. Algermissen, B. Askew, and A. Rogers of the USGS Golden, Colorado; and for the University of Utah Seismograph Stations for regional-network earthquake data. W. Nagy assisted in manuscript and figure preparation. M. Bauer, D. Galagher and S. Willett helped compile much of the geologic and geophysical information in the early stages of this project. D. Doser offered advice on the seismic moment methodology. G. Randall assisted with the initial compilation of earthquake data. Discussions with P. Lowman, NASA Goddard Space Flight Center regarding the objectives and geologic data were appreciated. J. Pechmann and W. P. Nash offered criticism and review of the manuscript.

1. Introduction

The Great Basin sub-province of the Basin-Range province, western U. S., is an area of active E-W lithospheric extension (Figure 1). Recognition of this strain regime has been inferred from many types of geologic and geophysical data summarized by Smith and Sbar (1974); Eaton, et al. (1978); Zoback, et al. (1981). Quantitative estimates of contemporary deformation and magnitudes of extension rates have been difficult to obtain, however various authors have made estimates of regional extension using studies of seismicity, fault plane geometries, intraplate tectonic models, and geodetic measurements (Proffett, 1977; Greensfelder et al., 1980; Minster and Jordan, 1984; Savage, 1983). In this study, the seismic moment tensor method was employed to determine strain and deformation rates of discrete areas of homogeneous strain and overall Great Basin opening rates. These data were then compared to strain rates estimated from geodetic measurements and to paleo-strain rates calculated from geologic data.

FIGURE 1 HERE

1.1 Strain rates from earthquake data.

Brittle strain release in the lithosphere is primarily expressed by earthquakes that can be used to assess regional strain (see for example Greensfelder et al. (1980); Doser and Smith, (1982,1983); Hyndman and Wiechert, (1983); Wesnousky, et al. (1982a). Earthquake magnitudes with fault plane orientations derived from fault plane solutions were used to determine the seismic moment tensors that in turn were used to calculate the strain rate tensor (Kostrov, 1974). Results of these

calculations provided data on strain and deformation rates that characterize the kinematics of Great Basin intraplate extension.

1.2 Cenozoic history of the Great Basin.

Great Basin extension began with the cessation of subduction along the west coast of North America about 30 mya. Prior to this extensional regime, Mesozoic volcanism was associated with subduction that produced a calc-alkaline volcanic arc. East of this arc, a foreland belt of folding and thrusting, associated with the Sevier and Laramide orogenies produced crustal compression and lithospheric shortening in areas that were later effected by late Cenozoic extension.

During the Miocene, about 30-40 mya, subduction was nearing its conclusion and WSW-ENE extension began in the Great Basin region, possibly as a result of back-arc spreading and stress relaxation of the lithosphere (Scholz et al., 1971; Zoback et al., 1981). A second period of regional Great Basin extension followed about 10-13 mya (Zoback et al., 1981), initially in the southern Basin-Range of Arizona and northern Mexico (Thompson and Burke, 1974). Marking the beginning of this extensional episode, the direction of extension rotated counterclockwise ~45° to a WNW-ESE direction (Zoback et al., 1981). Evidence from palinspastic reconstructions of reflection profiles in western Utah also implies these two periods of Great Basin extension (Von Tish et al., 1985).

Normal faulting that developed during the latter period of crustal extension has largely overprinted evidence for the earlier periods of extension and compression (Eaton et al., 1978). However, in some areas, contemporary strain may be accommodated by movement on pre-existing faults

developed during the early periods of deformation (Zoback and Zoback, 1980; Smith and Bruhn, 1984).

The Great Basin is still undergoing active E-W extension as evidenced by the province-wide seismicity and numerous normal-faulting fault plane solutions (Smith, 1978; Smith and Lindh, 1978; Zoback and Zoback, 1980). Some possible causes of this lithospheric extension have been suggested as pure crustal stretching, passive or active magmatic intrusion, crustal underplating, or a combination of these mechanisms (Lachenbruch and Sass, 1978). It appears that some mantle upwelling likely accompanied Great Basin extension to produce the wide-spread, Late Tertiary basaltic volcanism (Best and Hamblin, 1978), and the E-W symmetry of gravity and regional topography of the province (Eaton et al., 1978).

Great Basin topography is dominated by north-trending, normal-fault bounded ranges separated at 25 km average intervals by alluvium-filled basins. The region has generally high elevations from 1 km to 1.5 km and is characterized by high heat flow exceeding 90 mWm^{-2} (Lachenbruch and Sass, 1978), low Bouguer gravity (Eaton et al., 1978), a thin crust, 24-34 km, and low Pn velocities (Smith, 1978). The seismicity (Figure 2) occurs along diffuse bands up to 200 km wide with shallow focal depths (80% less than about 10 km) around its margins (Smith and Sbar, 1974).

FIGURE 2 HERE

1.3 Earthquake history of the Great Basin

Seismicity within the Great Basin (Figure 2) has been concentrated along the eastern province margin associated with the southern Intermountain Seismic

Belt (ISB); along the western province margin associated with the Sierra Nevada front, and in central Nevada (Smith, 1978). Large magnitude, M>6.5, Great Basin earthquakes have occurred principally in central Nevada, in Owens Valley, California, and at locations of pronounced changes in the trend of the southern ISB.

Great Basin seismicity has been characterized primarily by dip-slip and oblique-slip events throughout most of the region, including nine 6.5>M>7.3 normal faulting events that produced scarps (Smith, 1978; Smith and Lindh, 1978). Strike-slip and oblique-slip events have occurred along the region's southern and southwestern borders. Most earthquakes in the Great Basin occur at depths less than 15 km and 80% are generally less than 10 km (Smith and Sbar, 1974; Sibson, 1983; Smith and Bruhn, 1984).

Hypocenters of the largest, M7+, earthquakes, however, were located at greater depths, e.g. ~15 km (Smith and Richins, 1984), near the hypothesized brittle-ductile transition. The large magnitude, M7+, earthquakes can be clearly correlated with surface-breaking faults. However, for smaller earthquakes, generally less than M6.5, there is a lack of surface faulting.

It has been theorized that large earthquakes nucleate near the brittle-ductile transition where lithospheric loading is the principal contributor to deviatoric stress, but where strain rates, at $\sim 10^{-4} s^{-1}$ relieves the stored energy (Smith and Bruhn, 1984; Sibson, 1984). Smith and Bruhn's (1984) Great Basin rheological model suggests multiple brittle-ductile transition zones, where the multiplicity corresponds to changes in rock type with depth. The shallowest ductile zone is about 7 km deep, near the 80 percentile in focal depth distribution for the Wasatch and Sierra Nevada fronts.

The study area for this paper includes the intraplate extensional domains of the Basin and surrounding areas, principally southwestern Montana, western Wyoming, southeastern Idaho, eastern California, and southeastern Oregon (Figure 1). The transition from the Basin-Range to the San Andreas fault including the White Wolf, Lone Pine and Garlock faults was also included.

In summary, the objectives of the study were: 1) to determine the contemporary strain and deformation rates of this region of intraplate extension using the seismic moment tensor method; 2) to compare the contemporary strain rates with geodetically and geologically determined Quaternary strain rates, and 3) to assess the kinematics of Great Basin extension.

2. Strain determination from earthquake data

2.1 Strain rate calculation from the seismic moment tensor

The seismic moment method described here was used to calculate stresses, strains and seismic moments from earthquake magnitudes and fault plane solutions following the methods outlined by Kostrov (1974), Anderson (1979), Molnar (1979), and Doser and Smith (1982; 1983). The process involves the following steps:

1) Conversion of magnitudes to scalar moments - The seismic moment and seismic moment rates of a single fault are given by:

$$M_o = \mu A u \qquad (1a)$$

$$\dot{M}_o = \mu A \dot{u} \qquad (1b)$$

where M_o = seismic moment, u = displacement, A = fault plane area, μ = shear modulus, and $\dot{u}$ and $\dot{M}_o$ = slip rate and moment rate respectively (after Aki, 1966). Seismic moments can also be estimated from empirical moment-magnitude relationships and from inferred paleo-slip rates based upon dating of Quaternary faults. For this study, seismic moments for large earthquakes were taken from published sources, when possible; otherwise, the following moment-magnitude relations were used:

$$\log (M_o) = 1.1M_L + 18.4 \quad \text{Utah (extension, after Doser and Smith, 1982} \quad (2a)$$

$$\log (M_o) = 1.5M_L + 16.0 \quad \text{California (compressive strike-slip)} \quad (2b)$$

(Thatcher and Hanks, 1973).

Equation (2a) was applied to the Great Basin extensional and oblique-slip events and equation (2b) was used for the Great Basin-sourthern California transition, oblique and strike-slip events. The magnitudes were converted to the local (Richter) magnitude, M_L, scale.

The next step was to associate a regional stress field orientation with regions of homogeneous strain (Figure 3), to be defined later. The stress orientations from observed fault plane solutions for a given area were weighted and averaged, providing the average stress orientation. This direction was assumed for all earthquakes in a given area.

2) Calculate, sum and diagonalize moment tensors - The strike, dip and rake of the assumed fault plane for individual earthquakes was used to determine the moment tensor. The data for the fault plane, along with the scalar moment,

M_o, was used to find the moment tensor according to equations given by Aki and Richards (1980, pg. 106).

The moment tensor eigenvalues and the eigenvectors were then calculated. The eigenvalues compare to the principal stress values (Kostrov, 1974; Aki and Richards, 1980). The moment tensors of individual events were then summed, by component and the resulting regional moment tensors were diagonalized.

3) Strain and deformation rates - Assuming linear elasticity, the moment tensor can be converted to the strain-rate tensor using Kostrov's (1974) equation:

$$\dot{\varepsilon}_{ij} = \frac{\Sigma\, m_{ij}}{(2\mu\Delta V\Delta t)} \qquad (3)$$

$\delta\eta\varepsilon\theta\varepsilon$ ε_{ij} are the strain rate tensor components, m_{ij} are the moment tensor components. The summation represents the component summation of moments described above. ΔV is the volume of the lithospheric block defined by the surface dimensions of the homogeneous areas (Figure 3) and the estimated maximum depth of earthquake hypocenters at 15 km, Δt is the time difference between first and last events, and μ is the shear modulus assumed to be 3.3×10^{11} dynes/cm^2 (Molnar, 1979).

To find the maximum strain rates in the horizontal plane, the two-by-two strain-rate matrix (4) was then diagonalized.

$$\begin{matrix} \dot{\varepsilon}_{11} & \dot{\varepsilon}_{12} \\ \dot{\varepsilon}_{21} & \dot{\varepsilon}_{22} \end{matrix} \qquad (4)$$

Examples of the calculations and a detailed description of this method is given in Eddington (1985).

2.2 Homogeneous seismic source areas

One goal of this study was to determine detailed local and regional strain-rates. To determine local strain rates, Kostrov's method was applied to the smaller areas of assumed homogeneous strain release shown in Figure 3. The boundaries of the smaller areas were previously established by Renggli and Smith (1984) based on: 1) commonality of fault types and orientations such as shown in the paper by Greensfelder et al. (1980); 2) similarities of fault plane solution P and T axes (minimum and maximum principal stress axes); and 3) similarities in Quaternary geology. The three criteria were usually compatible, although an occasional fault plane solution displayed P and T axes inconsistent with area surface geology and other area fault plane solutions.

FIGURE 3 HERE

2.3 Limits and accuracy

The accuracy of the method described above is limited primarily by discretization approximations, incompleteness and/or vagueness in the earthquake catalogs and fault plane solution data, and incorrect magnitude-moment conversions.

The discrete area subdivisions described above, assume a volume of homogeneous strain. Although the area boundaries were chosen to enclose geologically and geophysically homogeneous regions, it is obvious that real strain fields are not completely homogeneous in discrete blocks, nor will they change magnitude and orientation discontinuously at block boundaries. Consequently, the area boundaries shown in Figure 3 could be misplaced up to

10-20 km introducing up to ± 5 percent error in strain magnitude and ± 15% error in strain direction.

Completeness of the earthquake data, particularly the percentage of events for which fault plane solutions have been determined, is a second limitation. The method requires that both a magnitude and a fault plane solution be given for each earthquake. The fault plane solution gives the principal stress orientation. Unfortunately, less than 1% of the earthquakes used were accompanied by fault plane solutions; however, most events of M 6+ in each area had solutions. The need for fault plane solutions for each earthquake was alleviated by averaging the stress orientations of the available fault plane solutions and applying the resulting "average fault plane solution" to each earthquake. This required an assumption of uniform strain release for all magnitude earthquakes. We know that in many areas of the Great Basin M <4 events produce a variety of fault plane orientations, sometimes not the same as for the larger, M>6, events in the same area. Since fault plane solutions for larger magnitude events were usually available and since larger events account for most of the seismic moment in any area (an increase of 1 in magnitude equals multiplying the moment by 10) the effect of this assumption on the accuracy of the strain rates is less than 5%.

Another limitation arises from variations in the type of magnitudes used, M_L, m_b, or M_S. The earthquake data in many of the older catalogs did not specify which magnitude scale was selected. The main earthquake file used here was a combination of several independently compiled catalogs. Simply treating all magnitudes the same would introduce significant error when they were converted to moments.

Fortunately, several independent sources were available that gave magnitude scales for many of these events. The U.S. Geological Survey, Great Basin Study provided a carefully prepared earthquake catalog that covered the period from 1900 to 1977 (Askew and Algermissen, 1983). Magnitude data from the University of Utah Seismograph Stations was correlated with USGS files and with published data on specific events (for example the work by Hanks et al. (1975) for California earthquakes) helped minimize the error caused by incorrect magnitude scale assumptions to be less than 10%.

Errors can also be introduced in the magnitude-moment conversion even if proper magnitude scales are assumed. Hanks and Boore (1984) suggested that different magnitude scales established for different parts of California are not really characteristic of different areas, but are dependent on the range of the earthquake magnitudes used to produce them. Their assertion is that log (moment) vs. magnitude is not a linear relationship, but that the magnitude of the slope of the curve increases with increasing earthquake magnitude. Thus, if only large magnitude earthquakes were used to establish a linear moment-magnitude relation, the slope of that line would be too steep and moments for small earthquakes would be underestimated. Conversely, if only smaller magnitude events were used, the slope would be small and the moments for larger earthquakes would be underestimated.

The primary moment-magnitude relation used in this study, equation (2a), (Doser and Smith, 1982) was based on spectral analyses of extensional earthquakes in Utah with magnitudes in the range M_L $3.7<M_L<6.6$ events would be accurately predicted by equation (2a). An earthquake magnitude outside this range might be converted inaccurately to a seismic moment. However, since smaller earthquakes have orders of magnitude less impact on the total moment

than largr events and since moments for most M_L>7 earthquakes were taken from independently determined results in the literature, possible nonlinearity of the moment-magnitude relation contributed less than 5% underestimation of moment in any given area.

TABLE 1 HERE

Since smaller earthquakes, with magnitudes M<4, are not included from earlier periods of recording this also adds to the seismic moment under-estimation. However, since large magnitude earthquakes contribute most of the moment, under-estimation from both incorrect magnitude-moment conversions and incomplete small earthquake listings was estimated to be less than 5%.

A more fundamental limitation of determining strain rates from earthquake data is the assumption of an idealized, brittle medium. There is evidence that at about 10-20 mya, the Great Basin stress field rotated about 45° (Zoback et al., 1981) from WSW-ENE to WNW-ESE. Re-activation of pre-existing faults by the present stress field could have introduced error into the results of this study. However, Kostrov's (1974) method, equation (3), assumes statistical distributions and orientations of dislocations in the deforming material. Hence, fault plane orientations for all events were not necessary for the calculation.

Another important limitation in moment-magnitude conversions is the variation in published seismic moment determinations for earthquakes. For example, Hanks et al. (1975) determined a moment for the 1952 Fort Tejon, California earthquake of 9.0×10^{17} dyne-cm, while Sieh (1977) gave a moment range of 5.0×10^{17} to 8.7×10^{17} dyne-cm for the same event. Variation in

recorded seismic moments can vary by a factor of three. This corresponds to possible error of ± 300 percent in strain rate calculations.

Seismic moments were taken from the results of other workers for 12 earthquakes (Table 1) ranging in magnitude from $6.1 < M < 7.9$. However, independent moments were not found for the large central Nevada earthquakes. The error in seismic moment determinations for large earthquakes using moment-magnitude relations may be a factor of three because of scatter in moment-magnitude curves. Hence, a ± 300 % error is possible whether the moment came from the literature or from a moment-magnitude relation.

The total possible error in strain and deformation rate calculations due to these limitations is ± 325% in magnitude and ± 15% in direction. The error in strain magnitude is almost entirely from uncertainty in seismic moment determination for large earthquakes, which exceeds all other sources of error.

3. Earthquake data

The earthquake catalog (Table 2) produced for this study contains a listing of the felt and instrumentally recorded earthquakes in the western U. S. Cordillera during the nineteenth and twentieth centuries up to and including much of 1981. Before 1962, earthquake recording was hampered by a lack of regional seismograph network coverage and the USGS file was the prime source of information. Only earthquakes recorded after 1900 were considered accurate enough and the files sufficiently complete for use in this study. Because of their large size and impact on the calculations, the 1857 M_s 8.3 Fort Tejon, California and the 1872 M_s 8.3 Owens Valley, California earthquakes were included in this study. All events including earthquakes within the Nevada nuclear test site were removed from the catalogs studied to

eliminate bias from the introduction of nuclear blasts that would not be distinguished from natural events.

TABLE 2 HERE

The record of post 1900, M>4 earthquakes was considered to be reasonably complete, since the number of M>4 events recorded in this century varies little from year to year. Figure 2a is a map of all $M \geq 4$ earthquakes within the study area. For example, in the study region, 3637 M>4 earthquakes produced a total seismic moment of 2.2×10^{28} dyne-cm; 572 M>5 events yielded 2.1×10^{28} dyne-cm; 80 M>6 events yielded 2.0×10^{28} dyne-cm; and 7 M>7 earthquakes produced 1.8×10^{28} dyne-cm. These data demonstrate that the 3630 earthquakes with magnitudes $4 < M < 7$ accounted for only 18% of the seismic moment released in all M>4 earthquakes; whereas the 7, M>7 earthquakes produced the remaining 82% of the moment.

The primary earthquake catalog was produced by choosing one file as the base, then comparing all other files to it. Events from other files that were not found in the key file were added to a master catalog. The final master file used the Askew and Algermissen (1983) Basin-Range file as a standard for correlation. Events were chronologically listed and duplicates were removed. The 1983 Borah Peak, Idaho, M_L7.3 earthquake and aftershocks were added from University of Utah files. For comparisons, when any two earthquakes had origin times closer than 10 seconds and epicenters closer than 15 km, they were considered duplicates and the master file location was used. Table 2 includes a list of the earthquake catalogs used in this compilation.

3.2 Cordilleran seismicity

The data used in this study included ~50,000 earthquakes out of the ~120,000 events summarized in the various catalogs. The area covered by the main earthquake data file extended from longitude 100°-130° W and from latitude 30° - 50° N. Figure 2a shows the seismicity confined primarily to the study area: ~longitude 109°30' W. to 125° W. and latitude 33°30' N to 46° N.

The areas of principal active seismicity occurred at or near locations of changes in direction of the ISB, along the Great Basin's western border, in central Nevada, and along the San Andreas fault and its associated faults. Almost half of the earthquakes studied were located in the San Andreas, Garlock, and White Wolf fault zones (in the Central California, Garlock, and Los Angeles areas). Figure 2d shows that, of the seven M7+ earthquakes that occurred in the study area, three were located in the Los Angeles, and Garlock areas; one M7+ event each occurred in the Owens Valley, California; West Central Nevada; Hebgen Lake/Yellowstone Park; and central Idaho areas.

3.4 Fault plane solutions

The fault plane solution data used in this study were compiled by Renggli and Smith (1984; and unpublished data) primarily from the data of Smith and Lindh's, (Table 5-1, 1978). These data were augmented by fault plane solutions for the M_L7.5, 1959, Hebgen Lake, Montana earthquakes (Doser, 1984); for the 1983, M_L7.3, Borah Peak earthquake sequence (Doser, 1985); and focal mechanisms of large Great Basin, pre-1964, earthquakes based on surface-wave analyses by Patton (1984). T-axes of these fault plane solutions are

presented in Figure 4 that show the direction of regional strain accompanying the earthquakes.

FIGURE 4 HERE

4. Contemporary strain rates

4.1 Strain rates from historic earthquakes

A summary of the moment tensor strain and deformation rates is presented in Tables 3 and 4 are shown in Figure 5. Time periods for given areas vary according to the data available but were generally from 1900 to 1981. Figure 5 also includes some of Anderson's (1979) results for southern California.

FIGURE 5 HERE

TABLE 3 HERE

TABLE 4 HERE

The general results show a principal east-west direction of extension for the seismically active parts of the Great Basin. E-W extension was dominant on the west edge of the Great Basin. In Idaho, Montana, and Wyoming, extension was accommodated by a large N-S component. In Utah, extension trended NW-SE. Some exceptions were in Provo, central Utah, and Utah-Nevada border areas (areas 18, 20, 21 and 23) where the principal horizontal strain corresponded to compression rather than extension. This pattern is consistent

with a rotation of the stress field from σ_1 approximately vertical and σ_2 and σ_3 in the horizontal plane, to σ_3 vertical and σ_1 and σ_2 in the horizontal plane. The central Wasatch front region (area 18) has had little earthquake activity in historic time and accordingly has a low deformation rate of only 0.001 mm/a, too small to be considered reliable. Also see Smith et al. (1984) for detailed discussion of strain rates in Utah.

The Colorado Plateau-Great Basin transition (area 20), may be influenced by the neighboring N-S compression of the northern Colorado Plateau. The central Utah area would seem geographically to be more closely associated with the Great Basin; however, here, the stress orientation of the area was determined primarily from a single event with a near-vertical nodal plane on the extreme eastern edge of the area. The stress orientation for the Utah-Nevada border area was dominated by a single large strike-slip event, M6.1, 1966. This solution is anomalous, hence the stress orientation may not be adequately accounted for. However, the strike-slip nature of this earthquake is the first of many that extend westward across southern Nevada.

The largest deformation rates were associated with the western margins of the Great Basin along the northern California-Nevada border (1.6 mm/a), in West-Central Nevada (7.5 mm/a), along the Walker Lane (2.9 mm/a), and in the Owens Valley (28.0 mm/a) (areas 3, 4, 5 and 7). Deformation in the Owens Valley area was exceptionally high because of the 1872, M_s 8.3, Owens Valley earthquake.

Another region of high strain rate occurred along the Great Basin's eastern border. Deformation rates of 1.0 to 4.7 mm/a were determined in areas where the trend of the ISB changes: for example in the Hebgen Lake/Yellowstone

Park; Hansel Valley, northern Utah; Central Utah; and Utah-Nevada border areas (areas 12, 15, 21 and 23).

Deformation of 2.0 mm/a in the Central Idaho area was due principally to the 1983, M_L7.3 Borah Peak, Idaho earthquake and aftershock and does not fit either of the two trends mentioned above. The central Idaho area may be associated with a northwest extension of the Great Basin eastern margin.

With the exception of the Owens Valley area, deformation rates in these rapidly deforming areas thus range from 1 to 9 mm/a; about 10 times greater than in other areas of the Great Basin. However, they were 10 times less than the 59 mm/a deformation rate calculated for the Garlock fault zone of southeastern California. Note that most of the Garlock area moment came from the 1857, M_S 8.3 Fort Tejon earthquake produced by fracture on the San Andreas fault along the south edge of the Garlock area.

4.2 Geodetically determined strain rates

Geodetic (trilateration and triangulation) networks have been used by several workers to determine strain rates. For purposes of comparison, Savage's (1983) summary of strain rates of different USGS trilateration networks was used along with modifications and additions taken from Savage et al. (1985), and Snay et al. (1984).

Some problems associated with geodetic determinations are inaccurate measurements because of inconsistent location of measurement stations and inconsistent measuring techniques. Also a factor in the usefulness of geodetic measurements is the sparseness of measurements throughout the western U. S., with the exception of California. A summary of deformation and strain rates derived from geodetic data are presented in Figure 6.

FIGURE 6 HERE

Geodetic strain rates were only available in about half of the areas considered in the seismic strain rate determinations. In many areas where geodetic strain measurements were available, strain and deformation rates were close to the values measured seismically. However, in some cases the geodetic rates were 10-20 times larger (Table 4).

Where geodetically determined strain rates were higher it was likely because seismically determined strains were from broader regions and thus represent spatial sampling differences. Geodetic networks were usually three to five times smaller than the areas used in this study and focused on the most actively deforming regions. Consequently, higher strain rates would be expected for geodetic network results.

The Walker Lane area (area 5) was an example of different areal coverage with different contemporary strain rates. The seismically and geodetically determined strain rates for this area, 1.3×10^{-16} sec^{-1} and $1.9 \times 10^{-15} sec^{-1}$ respectively, differ by almost an order of magnitude. However, the seismic and geodetic deformation rates for the area were 2.9 mm/a from earthquake data, and 3.6 mm/a measured geodetically (Savage, 1983). The earthquakes on the Excelsior fault were probably the source of most deformation in this area and were sampled by both methods. Thus, when area size discrepancies are eliminated, the resulting deformations agree within the accuracies of the methods.

5. Paleo-strain rates from geologic data

5.1 Paleo-strain determinations

Strain rates from geologic data (slip rates on faults) were determined using a conversion of fault slip-rates to seismic moment rates. Mapped slip rates and fault plane geometries were used to determine the scalar moment following the equation (1b). From this seismic moment rate, M_o, and the age of the fault displacement, strain rate can be found using:

$$\dot{\varepsilon} = \frac{\dot{M}_o \, k}{\mu \, l_1 \, l_2 \, l_3} \qquad (5)$$

(Anderson, 1979)

where l_1 = volume dimensions of the homogeneous seismic area, k = 0.75 an empirically determined constraint, (Doser and Smith, 1983) $\dot{\varepsilon}$ = scalar strain rate, and $\dot{M}_o$ = scalar moment rate. Moments for faults in the western U. S. (Figure 7) used here were calculated previously by Smith (1982) and unpublished data, assuming an average fault dip of 60°.

FIGURE 7 HERE

Fault slip data covered a range in ages of faulting from ~10,000 yr to 10 ma. Geologic displacement rates for the Wasatch front were determined from fault segmentation and slip rates by Schwartz and Coppersmith [1984]. Paleo-deformation rates calculated for areas in southern California by Anderson (1979) were also included in Figure 6. Results for the Borah Peak, Idaho earthquake area are from Scott et al. (1984).

Faults were grouped into the same areas as used in the seismic strain rate determination where possible. The seismic moment rates were summed following equation (5). Because of a lack of detailed information on the direction of fault slip, the direction of extension was assumed to be east-west for the Great Basin. North-south compression was assumed for areas associated with the San Andreas fault system (the Central California and Los Angeles areas) and in Idaho and Montana.

5.2 Accuracy of paleo-strain results

The primary limitation of the geologic data lie in its interpretation and in completeness. For the results to be complete, all faults with significant displacement must be included and assigned accurate slips, areas, and displacement ages. While there were numerous references to Holocene and Quaternary faults throughout the region, less than 30 percent had published slip rates. Fault dips at depth must also be accurately estimated since low-angle normal fault dips yield higher horizontal extension rate estimates. This study assumes a 60° average fault dip (Smith, 1982) but horizontal extension would increase by 1.5 for 40° fault dips.

Second, even if surface exposures of faults are adequate and all major faults have been studied in an area, only large earthquakes, M6.5+, will have produced surface displacements in the first place. Consequently, paleo-strain determinations in a given area would be underestimated.

Slip rate data in western Nevada and eastern California were so sparse that regional strain rate estimates are totally unreliable. The problem was less pronounced along the Intermountain Seismic Belt because of the intensive studies by Doser and Smith (1982; 1983).

5.3 Paleo-strain results

Paleo-deformation rates yield the highest values in two regions (Figure 8 and Table 5) Hebgen Lake, Montana-Yellowstone Park, 0.24 mm/a; and in western Wyoming, 0.74 mm/a. Here, the ISB changes from a N-S trend in Utah to a NNE-SSW trend in southeastern Idaho and western Wyoming. High deformation rates were also calculated for the central and southern Utah areas, 0.38 and 7.4 mm/a, where the ISB again changes trend from N-S in most of Utah to E-W in southeast Nevada. Seismic results offer a more reliable measure of strain concentration in these regions than do paleo-strain results.

Pre-historic slip-rate data for the west side of the Great Basin was considered incomplete resulting in unreliably low deformation rates. Figure 1 shows that both the east and west margins of the Great Basin are candidates for M>7 earthquakes and inherent high deformation yet insufficient data on mapped faults and slip rates exists to accurately assess pre-historic slip.

FIGURE 8 HERE

6. Comparisons of contemporary and paleo-strain rates

Table 4 demonstrates that paleo-strain rates are generally one to two orders of magnitude lower than contemporary strain rates. The exceptions to this pattern were: 1) the Los Angeles, California; western Wyoming, south Salt Lake, southern Utah, and northern Wasatch Front areas where the paleo-deformation rates of 49.3, 0.74, 0.03, 7.4, and 0.25 mm/a were significantly larger than seismically determined rates of 1.2, 0.07, 0.001, 0.23, and 0.04 mm/a; and 2) in the Idaho-Wyoming area, 0.14 versus 0.12 mm/a; central California, 4.0 versus 1.1; Cache Valley, Utah, 0.1 versus 0.3 mm/a; and the southern Wasatch front, 0.31 versus 0.13 mm/a areas where paleo-strain versus

seismically determined deformation rates were within a factor of four. These results suggest that historic seismicity and deformation in the above areas have been at lower than average levels, since the seismic values are no larger than the underestimated paleo-deformation values. It is also possible that these areas have more complete geologic data than other areas.

Paleo-strain rates in Figure 8 also show that deformation along the ISB, up to 7.4 mm/a in the Southern Utah area, was greater than along the western margins of the Great Basin with up to 0.08 mm/a in the west-central Nevada area. This result is the opposite of that determined using earthquake data where deformation rates along the ISB were as high as 2.8 mm/yr, in the Hebgen Lake/Yellowstone area, and deformation rates in the western half of the Great Basin were as high as 7.5 mm/yr in the west-central Nevada area. Again this difference is probably due to insufficient geologic data.

For comparison, Anderson (1979) calculated a deformation rate of 2.0 mm/a from geologic data in the Los Angeles area compared to 1.2 mm/a from the earthquake contribution. Likewise, he estimated deformation rates of 8.0 and 1.5 mm/a in the Garlock and Owens Valley, California areas where seismicity rates were 59.0 mm/a in the Garlock area and 28.0 mm/a in Owens Valley.

Comparisons of contemporary and paleo-deformation support the concept of anomalous Wasatch front low seismicity. The northern Wasatch Front area (area 16) contains the Wasatch fault, the primary surface-breaking fault of the eastern Great Basin. The northern Wasatch Front area is also bordered on the east and west by the seismically active Cache Valley and Hansel Valley areas. In contrast, the northern Wasatch front area has been seismically quiet throughout historic time. Less than 200 earthquakes have been recorded in that block in the last 78 years. The maximum magnitude earthquake to be recorded in the area during this time period was M_L=5.7.

Smith [1978] suggested that this "seismic gap" along the northern Wasatch fault is temporary and might be "filled" at a later time. The deformation rate from seismicity for the northern Wasatch Front was 0.04 mm/a and for the southern Wasatch Front, 0.13 mm/a. In contrast, the geologically determined rates were 0.25 mm/a and 0.31 mm/a, north and south. The higher paleo-deformation values suggest that contemporary seismic quiescence is indeed anomalous.

6.2 Comparisons of Great Basin extension rates

Overall Great Basin deformation patterns are used to assess the general kinematics of intraplate deformation in this region (Figure 9). Deformation and strain rates were calculated across the entire Great Basin along three profiles (B-B', B-B'' and C-C', Figure 9). The components of the deformation along the profiles were summed to give the integrated opening rate of the Great Basin.

FIGURE 9 HERE

Profile B-B', a line across northern California, Nevada, and northern Utah had a 10.0 mm/a deformation rate. Profile, B-B'', is an east-west line with an 8.4 mm/a rate. The southern line, C-C', is an east-west line across southeast California, southern Nevada, and southern Utah; here, the deformation rate diminishes to 3.5 mm/a. However, if the 1883 M_S8.3 Owens Valley earthquake is included and projected onto C-C', the deformation rate increases to 29.2 mm/a. The extension rates found along these profiles are summarized in Table 5. When strain rates were considered, it was found that B-B' experienced 2.7 x 10^{-16} sec^{-1}, B-B'' yielded 2.2 x 10^{-16} sec^{-1} and C-C'

yielded $1.4 \times 10^{-16} sec^{-1}$. The northern profiles displayed almost twice the strain rates of the southern profile, consistent with deformation rate results.

TABLE 5 HERE

The deformation rate in the northern Great Basin is more than twice as high as the southern Great Basin. This pattern implies fan shaped opening of the Great Basin similar to a pattern that was deduced from Cenozoic fault patterns by Wernicke, et al. (1982).

Earthquake induced deformation rates of 10.0 mm/yr on B-B' and 8.4 mm/yr on B-B'' determined along the two northern profiles shown in Figure 9 compare well with deformation rates determined from other studies. For example, Lachenbruch and Sass (1978) determined 5-10 mm/yr extension for the Great Basin using heat flow constraints and thermal models of extension.

Jordan et al., (1985) estimated a deformation rate across the Great Basin of equal to or less than 9 mm/yr (along profile A-A' in Figure 9) from North American-Pacific plate intraplate tectonic models, while the seismically determined deformation rate along line B-B'' was 8.4 mm/yr (Table 5)--a remarkable similarity for two different methods. This result implies that the North American-Pacific plate interaction, modeled by Jordan et al., (1985), may contribute a significant component to Great Basin extension. This comparison also leads to the conclusion that much of the Great Basin extension is expressed as earthquake-generated brittle fracture.

Geologically determined paleo-deformation rates established by other workers (Table 5) ranged from 1-20 mm/a, except for Proffett's (1977) deformation rate of about 200 mm/yr. A range of 1 to 20 mm/yr is consistent

with the deformation produced by contemporary seismicity. These comparisons suggest that since geologically inferred and contemporary strain rates are similar, the mechanism that facilitates Great Basin extension today operated throughout Quaternary times. Had the mechanism changed, we would expect to see greater differences in deformation rates between the contemporary and paleo-estimations.

Similar contemporary and paleo-strain rates in the Great Basin suggest that the seismic record, though experiencing short-term local variability, is a reasonable indicator of future seismicity on a regional scale. This conclusion is analogous to the findings of Wesnousky et al., (1982a, 1982b) for Japanese seismicity who found that contemporary variations in seismic activity were determined to be short-term effects that disappeared over periods of many hundreds of years.

8. Summary

This study has shown that, on a regional scale, contemporary strain rates from seismicity are comparable with strain rates determined from modern, geodetic measurements. Comparisons with paleo-strain rates determined from geologic data are however generally unreliable because of insufficient geologic data on slip rates.

Regionally, an E-W Great Basin maximum extension rate of 8 to 10 mm/a was determined from earthquake data. Locally, contemporary strain was concentrated at changes in direction of trend of the Intermountain Seismic Belt along the Great Basin eastern boundary; along the western margin of the Great Basin; in central Nevada, and in some other scattered areas primarily on region boundaries. Great Basin contemporary deformation rates in the range

1 to 28 mm/yr were found in this study. By comparison, rates of 20-50 mm/a were determined for active interplate subduction in the Pacific Northwest calculated from seismicity by Hyndman and Wiechert (1983). Likewise slip rates along the San Andreas fault ranged 45 to 55 mm/a based upon seismicity data (Anderson, 1979). Thus, Great Basin deformation rates from seismicity were, on average, from 2 to 10 times lower than plate convergence rates.

Patterns of seismicity and high deformation rates of the Great Basin show that most brittle fracture occurs along its margins and along the Central Nevada seismic belt. The stress release and accompanying crustal fracture represented by this seismicity may have accommodated magma ascension through the lithosphere, in some cases reaching the surface. Figure 10, is a map of Quaternary volcanism for the last 5 ma (Smith and Luedke, 1984; Wernicke et al., 1986) and the seismically determined deformation rates of this study. These data suggests that brittle fracture and subsequent magma intrusion has persisted concomittantly along the edges of the Great Basin for at least the last few million years.

FIGURE 10 HERE

The local and regional deformation rate results, summarized above, imply that brittle fracture has been produced as the principal strain release mechanism, although it may ultimately be driven by creep and flow at lower lithospheric depths. It follows that most Great Basin extension has thus been expressed as brittle fracture in the upper crust and that creep in the whole of the lithosphere probably does not exceed that of brittle strain.

References Cited

Aki, K., Generation and propagation of G waves from the Nigata earthquake of June 16, 1964 2. Estimation of earthquake moment, release energy, and stress drop from the G-wave spectrum, Bull. of the Earthquake Res. Inst. Tokyo Univ., 44, 73-88, 1966.

Aki, K. and P. Richards, Quantitative Seismology, pp. 105-119, W. H. Freeman San Francisco, Calif., 1980.

Anderson, J. G., Estimating the seismicity from geological structure for seismic-risk studies, Bull. Seismol. Am., 69, 135-158, 1979.

Askew, B. and S. T. Algermissen, An earthquake catalog for the Basin and Range province 1803-1977, U.S. Geol. Surv. Open-File Rep., 83-86, 1983.

Davis, G. A., Problems of intraplate extensional tectonics western United States: in Continental Tectonics, Nat. Acad. Sci. Wash., D. C., 84-95, 1980.

Doser, D. I., Source parameters and faulting processes of the August 1959 Hebgen Lake, Montana earthquake sequence, Ph.D dissertation, 152 pp., University of Utah, Salt Lake City, Utah, 1984.

Doser, D. I., Source parameters and faulting processes of the 1959 Hebgen Lake, Montana earthquake sequence, J. Geophys. Res., 90, 4537-4556, 1985.

Doser, D. I. and R. B. Smith, Seismic moment rates in the Utah region, Bull. Seismol. Soc. Am., 72, 525-551, 1982.

Doser, D. I. and R. B. Smith, Seismicity of the Teton-Southern Yellowstone Region, Wyoming, Bull. Seism. Soc. America, 73, 1369-1394, 1983.

Eaton, G. P., R. R. Wahl, H. J. Prostka, D. R. Mabey and M. D. Kleinkopf, Regional gravity and tectonic patterns: Their relation to late Cenozoic epeirogeny and lateral spreading in the western Cordillera; in Cenozoic Tectonics and Regional Geophysics of the Western Cordilleran, R. B. Smith and G. P. Eaton (eds.), Mem. Geol. Soc. Am., 152, 51-91, 1978.

Eddington, P. K., Kinematics of Great Basin intraplate extension from earthquake, geodetic and geologic information, unpublished M.S. thesis, University of Utah, Salt Lake City, Utah, 1985.

Greensfelder, R. W., Kintzer, F. C. and M. R. Somerville, Seismotectonic regionalization of the Great Basin, and comparison of moment rates computed from Holocene strain and historic seismicity: summary, Bull. Geol. Soc. Am., 97, 518-523, 1980.

Hamilton, W., and W. B. Myers, Cenozoic tectonics of the western United States, Rev. Geophys., 4, 509-549, 1966.

Hanks, T. C., and D. M. Boore, Moment-magnitude relations in theory and practice, J. Geophys. Res., 89, 6229-6235, 1984.

Hanks, T. C., J. A. Hileman and W. Thatcher, Seismic moments of the larger earthquakes of the southern California region, Geol. Soc. Am. Bull., 86, 1131-1139, 1975.

Hyndman, R. D. and D. H. Wiechert, Seismicity and rates of relative motion on the plate boundaries of western North America, Geophys. J. R. Astr. Soc., 72, 59-82, 1983.

Jordan, T. H., J. B. Minster, D. C. Christodoulidis and D. E. Smith, Constraints on western U. S. deformation from satellite laser ranging, preprint, 1985.

Kostrov, V. V., Seismic moment and energy of earthquakes, and seismic flow of rock, Izv. Earth Phys., 1, 23-40, 1974.

Lachenbruch, A. H., Heat flow in the Basin and Range province and thermal effects of tectonic extension; Pageoph., 117, 34-50, 1979.

Lachenbruch, A.H. and J. H. Sass, Models of an extending lithosphere and heat flow in the Basin and Range province; in Cenozoic Tectonics and Regional Geophysics of the Western Cordillera, R. B. Smith and G. P. Eaton (eds), Mem. Geol. Soc. Am., 152, 209-250, 1978.

Minster, J. B. and T. H. Jordan, Vector constraints on Quaternary deformation of the western United States east and west of the San Andreas fault, in Crouch, J. K., and Barbman, S. B., eds., Tectonics and Sedimentation along the California margin, Pacific Sect. Soc. Econ. Paleontologists Mineralogists, 38, 1-16, 1984.

Molnar, P., Earthquake recurrence intervals and plate tectonics, Bull. Seismol. Soc. Am., 69, 115-133, 1979.

Patton, H. J., P-wave fault-plane solutions and the generation of surface waves by earthquakes in the Western United States, preprint, 1984.

Proffett, J. M., Jr., Cenozoic geology of the Yerington district, Nevada and implications for the nature of and origin of Basin and Range faulting, Bull. Geol. Soc. Am., 88, 247-266, 1977.

Renggli, C. and R. B. Smith, Estimates of crustal extension for the Basin-Range/southern San Andreas associated with active seismicity (abstract), Earthquake Notes, 55, 29, 1984.

Savage J. C., Strain accumulation in western United States, Ann. Rev. Earth Planet. Sci., 11, 11-43, 1983.

Savage, J. C., M. Lisowski and W. H. Prescott, Strain accumulation in the Rocky Mountain states, J. Geophys. Res., 1985.

Scholz, C. H., M. Barazangi and M. L. Sbar, Late Cenozoic evolution of the Great Basin, Western United States, as an ensialic interarc basin, Geol. Soc. Am. Bull., 82, 2979-2990, 1971.

Schwartz, D. P. and K. J. Coppersmith, Fault behavior and characteristic earthquakes: Examples from the Wasatch and San Andreas fault zones, J. Geophys. Res., 89, 5681-5698, 1984.

Scott, W. E., K. L. Pierce and M. H. Hait, Jr., Quaternary tectonic setting of the 1983 Borah Peak earthquakes, Central Idaho, preprint, 1984.

Sibson, R. H., Fault zone models, heat flow, and the depth distribution of earthquakes in the continental crust of the United States, Bull. Seismol. Soc. Am., 72, 151-163, 1983.

Sieh, K. E., A study of Holocene displacement history along the south-central reach of the San Andreas fault, Ph.D. thesis, Stanford Univ., Stanford, California, 1977.

Smith, R. B., Seismicity, crustal structure, and intraplate tectonics of the interior of the western Cordillera, in Cenozoic Tectonics and Regional Geophysics of the Western Cordillera, R. B. Smith and G. P. Eaton (eds), Mem. Geol. Soc. Am., 152, 111-144, 1978.

Smith, R. B., Intraplate seismo-tectonics and mechanisms of extension in the western United States, Abs., AGU Chapman Conference on Fault Behavior and Earthquake Generation Process, Snowbird, Utah, 1982.

Smith, R. B., and M. Sbar, Contemporary tectonics and seismicity of the western United States with emphasis on the Intermountain Seismic Belt, Bull. Geol. Soc. of Am., 85, 1205-1218, 1974.

Smith, R. B. and A. G. Lindh, Fault-plane solutions of the western United States: a compilation, in Cenozoic Tectonics and Regional Geophysics of the Western Cordillera, R. B. Smith and G. P. Eaton (eds), Mem. Geol. Soc. Am., 152, 107-109, 1978.

Smith, R. B. and R. L. Bruhn, Intraplate extensional tectonics of the eastern Basin-Range: Inferences on structural style from seismic reflection data, regional tectonics and thermal-mechanical models of brittle/ductile deformation, J. Geophys. Res., 89, 5733-5762, 1984.

Smith, R. B. and W. Richins, Seismicity and earthquake hazards of Utah and the Wasatch Front: Paradigm and paradox, U.S. Geol. Surv. Open-File Rep., 84-763, 73-112, 1984.

Smith, R. B., P. Eddington and L. L. Lillian Leu, Strain Rates in Utah from Seismic Moments, Paleoslip, and Geodetic Surveys, U.S. Geol. Surv. Open-File Rep., 84-763, 422-437, 1984.

Smith, R. L. and R. G. Luedke, Potentially active volcanic lineaments and loci in western conterminous United States, in Explosive Volcanism: Inception, Evolution, and Hazards, pp. 47-66, Nat. Res. Counc., National Academy Press, Wash. D.C., 1984.

Snay, R. A., R. B. Smith and T. Soler, Horizontal strain across the Wasatch Front near Salt Lake City, Utah, J. Geophys. Res., 89, 1113-1122, 1984.

Stewart, J. H., Basin and Range structure in western North America: A review, in Cenozoic Tectonics and Regional Geophysics of the Western Cordillera, R. B. Smith and G. P. Eaton (eds.), Mem. Geol. Soc. Am. 152, 1-13, 1978.

Thatcher, W. and T. C. Hanks, Source parameters of southern California earthquakes, J. Geophys. Res., 78, 8547-8576, 1973.

Thenhaus, P. C., and C. M. Wentworth, Map showing zones of similar ages of surface faulting and estimated maximum earthquake size in the Basin and Range province and selected adjacent areas, U.S. Geol. Surv. Open-File Rep., 82-742, 1982.

Thompson, G. A. and D. B. Burke, Regional geophysics of the Basin and Range province, A. Rev. Earth Planet Sci., 2, 213-238, 1974.

Von Tish, D. B., R. W. Allmendinger and J. W. Sharp, History of Cenozoic extension in central Sevier Desert, west-central Utah, from COCORP seismic reflection data, Bull. Am. Assoc. Petrol. Geol., 69, 1077-1087, 1985.

Wallace, R. E., Patterns of faulting and seismic gaps in the Great Basin province: in Proc. Conf. VI, Methodology for Identifying Seismic Gaps and Soon-to-Break Gaps, U.S,. Geological Survey, Open-File Rep. 78-943, 1978.

Wernicke, B. P., J. E. Spencer, B. C. Burchfiel and P. L. Guth, Magnitude of extension in the southern Great Basin, Geology, 10, 499-502, 1982.

Wesnousky, S. G., C. H. Scholz and K. Shimazaki, Deformation of an island arc: Rates of moment release and crustal shortening in intraplate Japan determined from seismicity and Quaternary fault data, J. Geophys. Res., 87, 6829-6852, 1982a.

Wesnousky, S. G., C. H. Scholz, K. Shimazaki and T. Matsuda, Earthquake frequency distribution and the mechanics of faulting, J. Geophys. Res., 88, 9331-9340, 1982b.

Wright, L., Late Cenozoic fault patterns and stress fields in the Great Basin and westward displacement of the Sierra Nevada block, Geology, 4, 489-494, 1976.

Zoback, M. L. and M. D. Zoback, State of stress in the conterminous United States, J. Geophys. Res., 85, 6113-6156, 1980.

Zoback, M. L., R. E. Anderson and G. A. Thompson, Cainozoic evolution of the state of stress and style of tectonism of the Basin and Range province of the Western United States, Philos. Trans. R. Soc. London Ser. A., 300, 407-434, 1981.

Table 1. Seismic moments for large earthquakes of the Great Basin and surrounding region.

Earthquake		Magnitude	Moment dyne-cm	Reference
California	Jan 9, 1857	M_s8.3	5.3-8.7x10^{27}	Sieh (1977)
			9.0x10^{27}	Hanks et al., (1975)
	March 26, 1872	M_s8.3	5.0x10^{26}	Hanks et al., (1975)
	March 15, 1946	M_L6.0	1.0x10^{25}	Hanks et al., (1975)
	July 21, 1952	M_L7.7	2.0x10^{27}	Hanks et al., (1975)
	July 21, 1952	M_L6.0	3.0x10^{25}	Hanks et al., (1975)
	July 29, 1952	M_L6.0	3.0x10^{25}	Hanks et al., (1975)
	Feb 9, 1971	M_L6.4	1.0x10^{26}	Hanks et al., (1975)
Utah	1934	M_L6.6	7.7x10^{25}	Doser and Smith (1982)
Hebgen Lake	1959	M_L7.5	1.0x10^{27}	Doser (1985)
Idaho	1975	M_L6.2	1.5x10^{25}	Doser (1985)
Yellowstone	1975	M_L6.1	7.5x10^{24}	Doser (1985)
Borah Peak	1983	M_L7.3	3.3x10^{26}	Doser (1985)

Table 2. Earthquake data, periods of data coverage and sources.

	Period of Time Covered	Source
1.	1900 - 1981 including 1983 Borah Peak, Idaho data	University of Utah Seismograph Stations, Salt Lake City
2.	1900 - 1980 possible gaps from 1900 - 1970	University of Nevada Network, Reno
3.	1928 - 1980 1900 - 1973 1900 - 1974 1910 - 1974	National Geophysical Solar Terrestrial Data Center - Four files used PDE (USCGS-USGS) Oregon State University Division of Mines and Geology (California) University of California at Berkeley
4.	1932 - 1981 Preliminary determinations of epicenters for 1975 - 1977 and for 1980 - 1981	California Institute of Technology Southern Network
5.	Aug. 1978 - Jan. 16, 1982	USGS, Southern Basin and Range Network
6.	July 26, 1974 - Nov. 10, 1978	Montana earthquake data from "Historical seismicity and earthquake hazards in Montana"
7.	1969 - Nov. 30, 1981	USGS, southern California Network, Menlo Park, California - summary data
8.	Jan. 1, 1973 - June 30, 1980	University of California Network, Berkeley, California
9.	1900 - 1977	USGS Great Basin file, USGS open file report 83-86, 1983)

Table 3. Number of earthquakes, maximum magnitude (M_{max}), principal moment tensor component (M_1), horizontal deformation rates, and maximum horizontal strain rates for homogeneous areas of the Great Basin

Area No.	Area Name	Number of earthquakes	M_{max}	M_1 (dyne-cm/a)	Horizontal Deformation (mm/a)	Strain Rate (sec^{-1})
1.	Oregon-Nevada Border	71	$5.0M_S$	$2.3x10^{23}$	0.2	$2.4x10^{-17}$
2.	Oroville	590	$6.0M_S$	$7.6x10^{23}$	0.5	$8.6x10^{-17}$
3.	Northern California-Nevada Border	1429	$6.4M_L$	$1.7x10^{24}$	1.6	$2.1x10^{-16}$ N90°W
4.	West-Central Nevada	2533	$7.8M_L$	$1.9x10^{25}$	7.5	$1.0x10^{-15}$ N69°W
5.	Walker Lane	2237	$6.0M_L$	$1.8x10^{24}$	2.9	$9.6x10^{-17}$ N46°W
6.	Southeast Nevada	118	$6.0m_b$	$5.5x10^{23}$	0.22	$9.6x19^{-17}$ N22°W
7.	Owens Valley	3809	$8.3M_S$	$4.9x10^{25}$	28.0	$3.7x10^{-15}$ N83°E
8.	Central California	20827	$6.9M_L$	$3.3x10^{24}$	1.1	$1.8x10^{-16}$ N19°E
9.	Garlock	5647	$8.3M_S$	$8.9x10^{25}$	59.	$6.8x10^{-15}$ N13°W
10.	Los Angeles	4175	$6.3M_L$	$2.4x10^{24}$	1.2	$1.8x10^{-16}$ N27°W
11.	Central Idaho	918	$7.3M_L$	$4.5x10^{24}$	2.0	$3.3x10^{-16}$ N29°E
12.	Hebgen Lake	1332	$7.6M_L$	$4.5x10^{24}$	4.7	$1.1x10^{-15}$ N11°E
13.	Western Wyoming	1159	$4.5M_L$	$6.7x10^{22}$	0.07	$1.4x10^{-17}$ N41°W
14.	Soda Springs	242	$5.0M_L$	$1.9x10^{23}$	0.12	$2.7x10^{-17}$

Table 3 (continued)

Area No.	Area Name	Number of Earthquakes	M_{max}	M_1 (dyne-cm/yr)	Horizontal Deformation (mm/yr)	Strain Rate (sec^{-1})
15.	Hansel Valley	1944	$6.8M_L$	$1.8x10^{24}$	1.5	$6.3x10^{-16}$ N67°E
16.	Northern Wasatch Front	166	$5.7M_L$	$7.9x10^{22}$	0.04	$3.8x10^{-17}$ N78°E
17.	Cache Valley	789	$5.9M_L$	$41.x10^{23}$	0.29	$1.3x10^{-16}$ N79°W
18.	South Salt Lake	141	$5.4M_L$	$3.7x10^{21}$	0.001	$-4.x10^{-19}$ N66°W
19.	Southern Wasatch Front	520	$5.7M_L$	$1.7x10^{23}$	0.13	$1.3x10^{-16}$ N76°E
20.	Provo	249	$5.7M_L$	$3.2x10^{22}$	0.06	$1.5x10^{-17}$ N37°E
21.	Central Utah	962	$6.9M_L$	$2.2x10^{24}$	1.3	$2.6x10^{-16}$ N35°W
22.	Southern Utah	234	$5.5M_L$	$1.5x10^{23}$	0.23	$4.5x10^{-17}$ N59°E
23.	Utah - Nevada Border	94	$6.3M_L$	$5.8x10^{23}$	1.0	$4.5x10^{-16}$ N64°E

Table 4. Comparison of strain and deformation rates using geologic (paleo-earthquake), contemporary seismicity and geodetic data.

Area	Geologic		Earthquake		Geodetic	
	Deformation Rate (mm/a)	Strain Rate (sec^{-1})	Deformation Rate (mm/a)	Strain Rate (sec^{-1})	Deformation Rate (mm/a)	Strain Rate (sec^{-1})
Oregon-Nevada Border			0.19	2.4×10^{-17}		
Oroville, California			0.5	8.6×10^{-17}		
Northern California-Nevada Border	0.02	2.6×10^{-18}	1.6	2.1×10^{-16}		
West-central Nevada	0.08	1.3×10^{-17}	7.5	1.0×10^{-15}	2.0	1.6×10^{-15}
Walker Lane, Southeast Nevada	0.001	3.8×10^{-19}	2.9	1.3×10^{-16}	3.6	1.9×10^{-15}
			0.22	9.6×10^{-17}		
Owens Valley			28.0	3.7×10^{-15}	2.5	2.5×10^{-15}
Central California	4.0	-1.9×10^{-16}	1.1	-1.8×10^{-16}	1.8	-2.9×10^{-15}
Garlock	2.5	4.4×10^{-16}	59.	-6.8×10^{-15}	11.2	-5.1×10^{-15}
Los Angeles	49.3	-1.1×10^{-14}	1.2	-1.8×10^{-16}	13.5	-4.8×10^{-15}
Central Idaho*	0.08	1.3×10^{-17}	2.0	3.3×10^{-16}		
Hebgen Lake/Yellowstone Park	0.24	3.5×10^{-17}	4.7	1.1×10^{-15}	11.2	8.9×10^{-15}
Western Wyoming	0.74	2.9×10^{-16}	0.07	1.4×10^{-17}		
Soda Springs	0.14	3.8×10^{-17}	0.12	2.7×10^{-17}		
Hansel Valley	0.11	4.8×10^{-17}	1.5	6.3×10^{-16}		
Northern Wasatch Front	0.25	1.9×10^{-16}	0.04	3.8×10^{-17}	0.6	3.2×10^{-16}
Cache Valley	0.10	4.4×10^{-17}	0.29	1.3×10^{-16}		
South Salt Lake	0.03	1.3×10^{-17}	0.001	-4.1×10^{-19}		
Southern Wasatch Front	0.31	2.4×10^{-16}	0.13	1.3×10^{-16}		
Provo	0.03	1.2×10^{-17}	0.06	-1.5×10^{-17}		
Central Utah	0.38	1.2×10^{-16}	1.3	-2.6×10^{-16}		
Southern Utah	7.4	9.8×10^{-16}	0.23	4.5×10^{-17}		
Utah-Nevada Border			1.0	-4.5×10^{-16}		

* from Scott et al. (preprint, 1984)

Table 5. Great Basin strain rates, deformation rates, and total extension from this and other studies

Reference	Strain Rate (sec^{-1})	Deformation Rate (mm/a)	Total Extension(%)
This Study			
Profile B-B'	2.6×10^{-16}	10.0	~10
B-B'	2.2×10^{-16}	8.4	~10
C-C'	1.3×10^{-16}	3.5	~10
Other Studies			
Jordan et al. (1985)			
A-A'		< 9	
Wright (1976)			
north		5.8 - 7.5	~10
south		3.7 - 10.1	10-50
Profett (1977)		200	30-35
Thompson and Burke (1974)	3.2×10^{-16}	8	~10
Eaton et al. (1978)	3.2×10^{-16}	8	~10
Zoback et al. (1981)			15-39
Minster and Jordan (1984)			
Geology[1]		3-20	
heat flow[2]		3-12	
paleo-seismicity[3]		1-12	
seismicity[4]		5-22	

[1] Hamilton and Myers (1966), Stewart (1978), Davis (1980), Profett (1977)

[2] Lachenbruch (1979), Lachenbruch and Sass (1978)

[3] Wallace (1978), Thompson and Burke (1974), Greensfelder et al., (1980)

[4] Greensfelder et al., (1980), Anderson (1979)

FIGURE CAPTIONS

Fig. 1. Active fault map of Great Basin study area (inner area). Faults of Late Cenozoic age are principally of Quaternary age. Data taken from published and unpublished sources (references on file at the University of Utah).

Fig. 2. Earthquake epicenter maps from regional network and historic data compiled for this study. Data covered the period, 1900-1981 including the 1983, Borah Peak, Idaho earthquake sequence: a) $M_L > 4$; b) $M_L > 5$; c) $M_L > 6$, and d) $M_L > 7$.

Fig. 3. Map of sub-regions of assumed homogenous strain.

Fig. 4. Map of T (tension) axes from fault plane solution of the Great Basin. Data taken from Smith and Lindh (1978); Doser (1984); Kienle and Couch (unpublished data, 1977); and Patton (1984).

Fig. 5. Great Basin seismically determined strain/deformation rates. In each area, top value is deformation rate in mm/a, bottom value is strain rate in s^{-1}; second number is power of 10; * from Hyndman and Wiechert (1983). # from Anderson (1979).

Fig. 6. Western U.S. geodetically determined extensional deformation and strain rates. The top number is deformation rate (mm/a) and the bottom is strain rate (s^{-1}). The second number is power of 10. Data are from Savage (1983), Savage et al. (1985), and Snay et al. (1984).

Fig. 7. Location of faults with Late Cenozoic displacement rates used in this study. Data from Smith (unpublished data, 1982), and Thenhaus and Wentworth (1982). Crosses, +, indicate centers of mapped faults for which slip rates were available.

Fig. 8. Great Basin paleo-strain and deformation rates from geologic data. Top value is deformation rate in mm/a; bottom value is strain rate in s^{-1}; second number is power of 10. See Figure 5 for comparison.

Fig. 9. Great Basin regional extension. A-A' is from Jordan et al. (1985) intraplate kinematic model of motion between North American and Paific plates constrained by satellite ranging data; B-B', B-B", and C-C' from this study. Value in parentheses below C-C' include deformation from the Owens Valley, California.

Fig. 10. Western U.S. volcanism and seismically determined deformation rates. Volcanism is from Smith and Luedke (1984) and deformation rates are in mm/a.

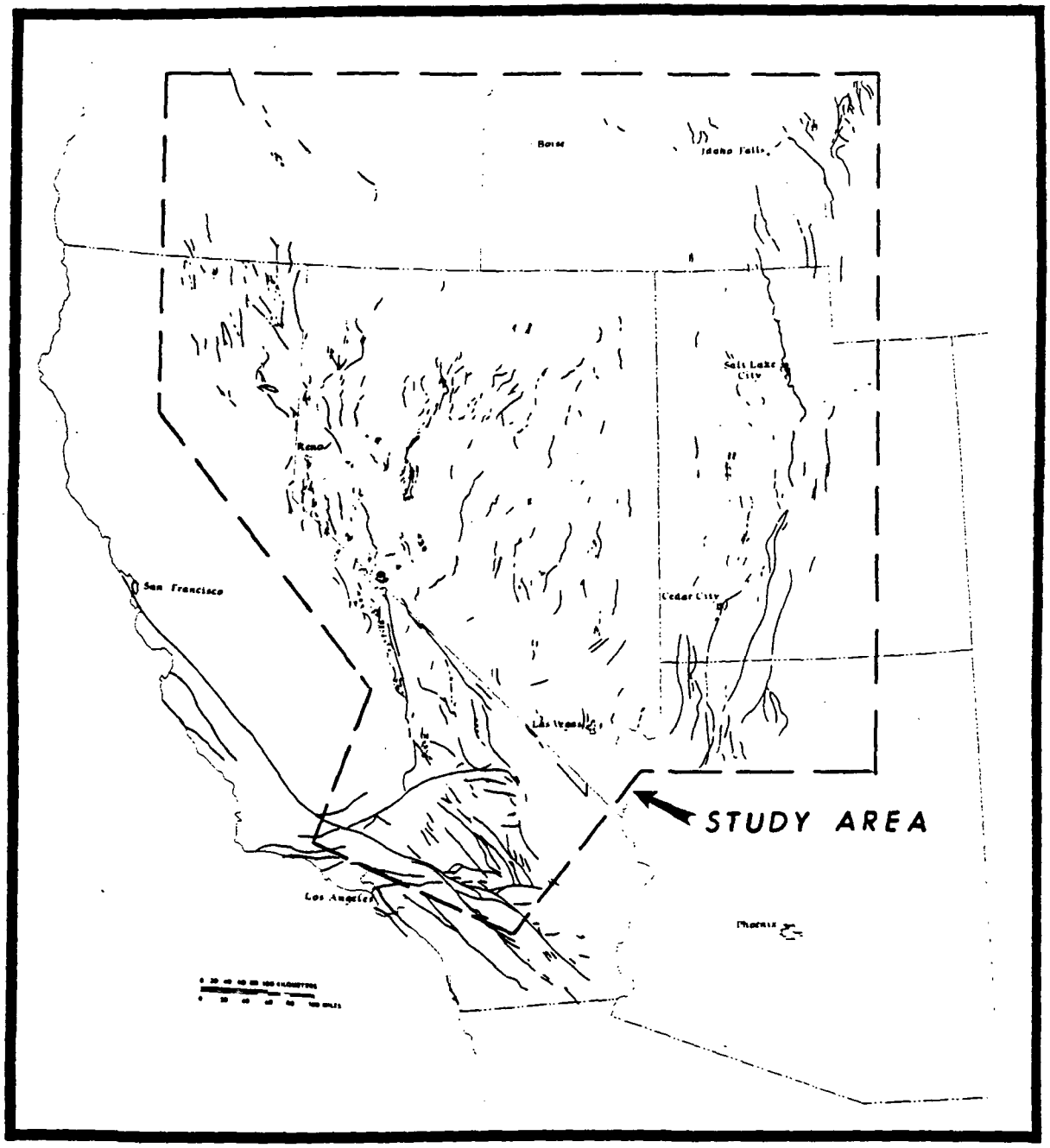

FIG. 1 Eddington et al.

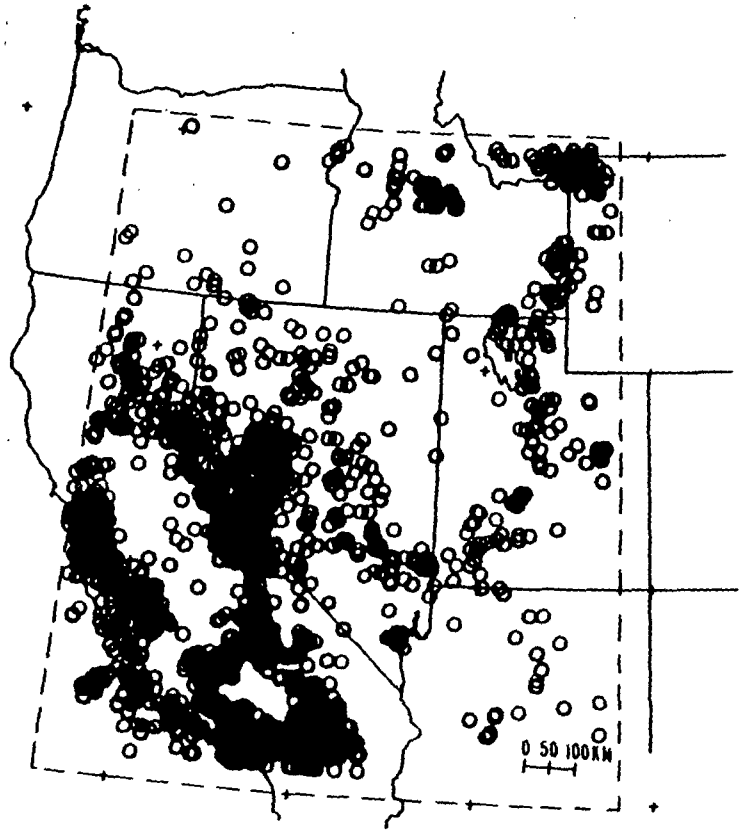

a) Magnitude 4+ Epicenter Map

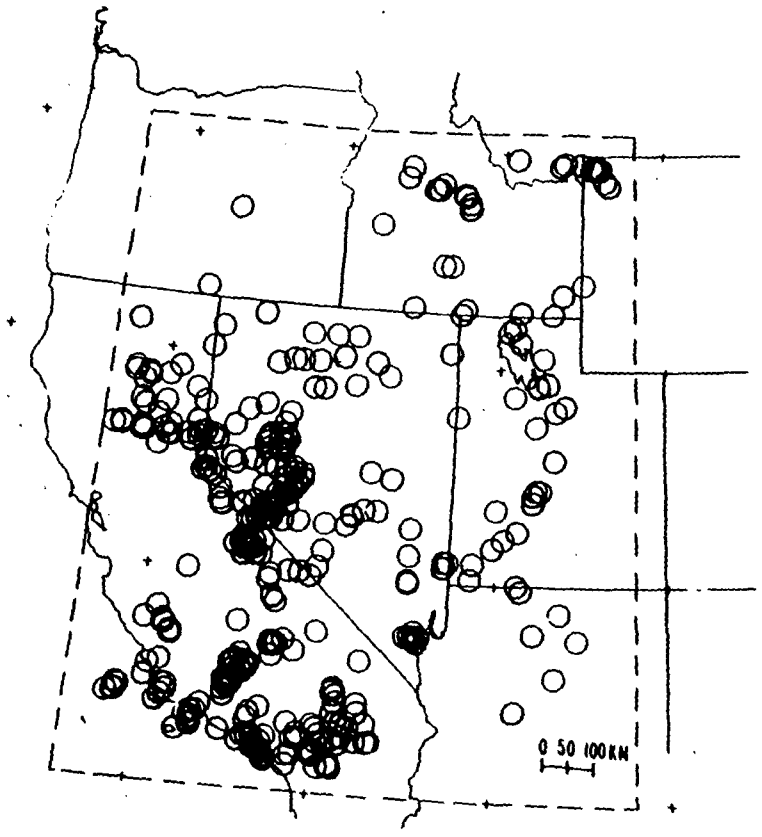

b) Magnitude 5+ Epicenter Map

FIG 2 Eddington et al.

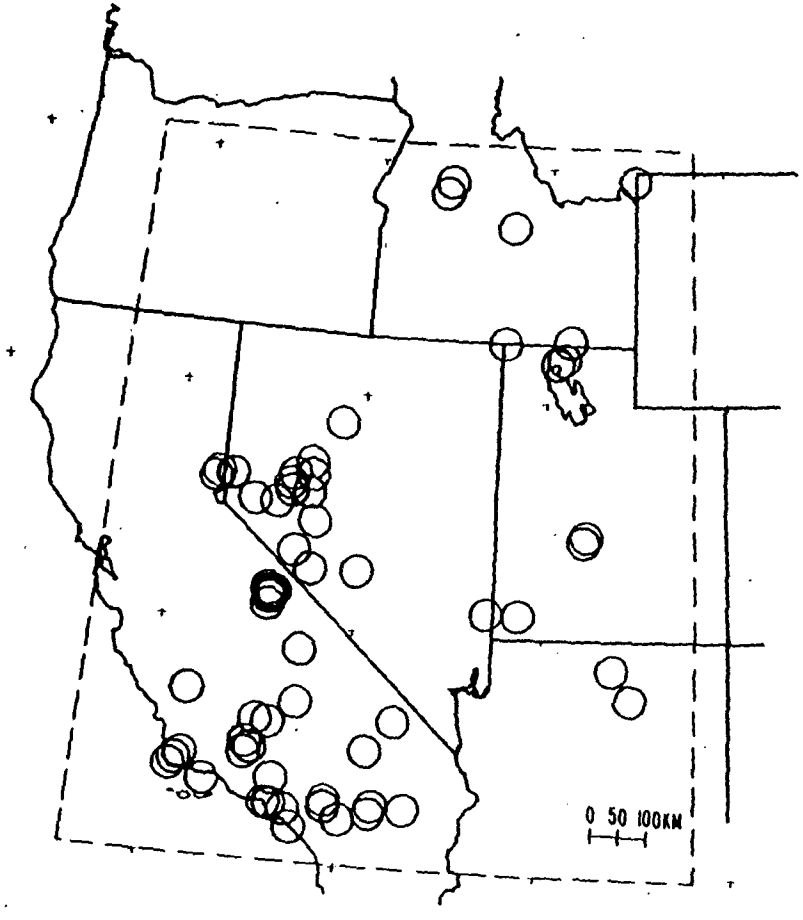

c) Magnitude 6+ Epicenter Map

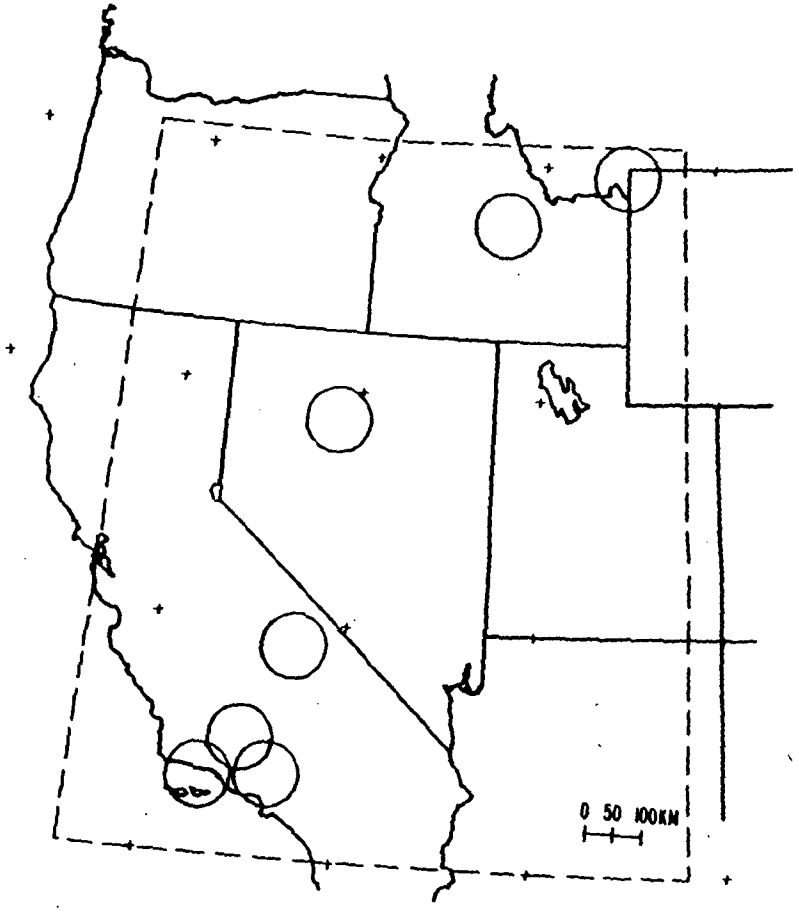

d) Magnitude 7+ Epicenter Map

FIG 2 Eddington et al.

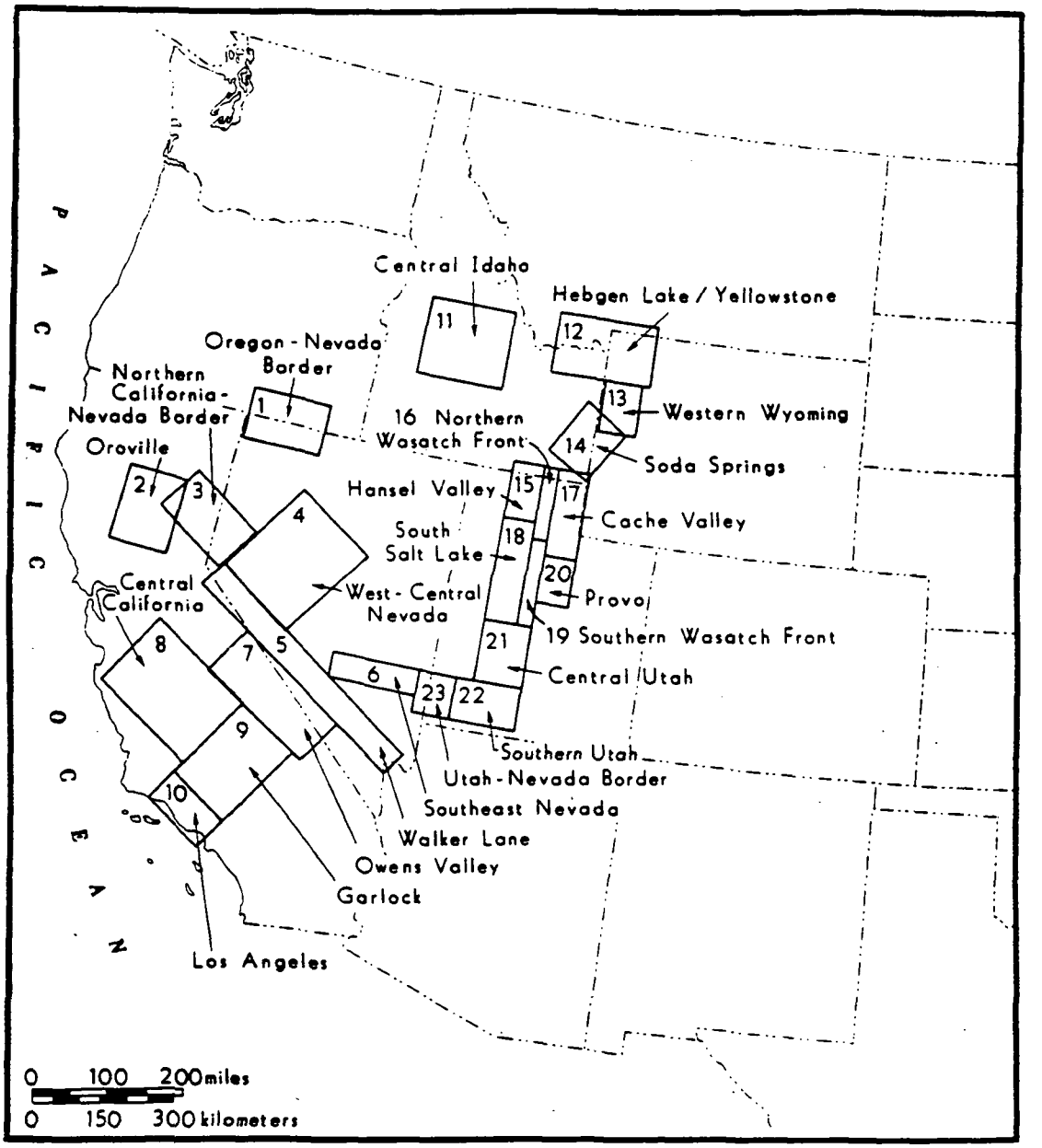

FIG 3 Eddington et al

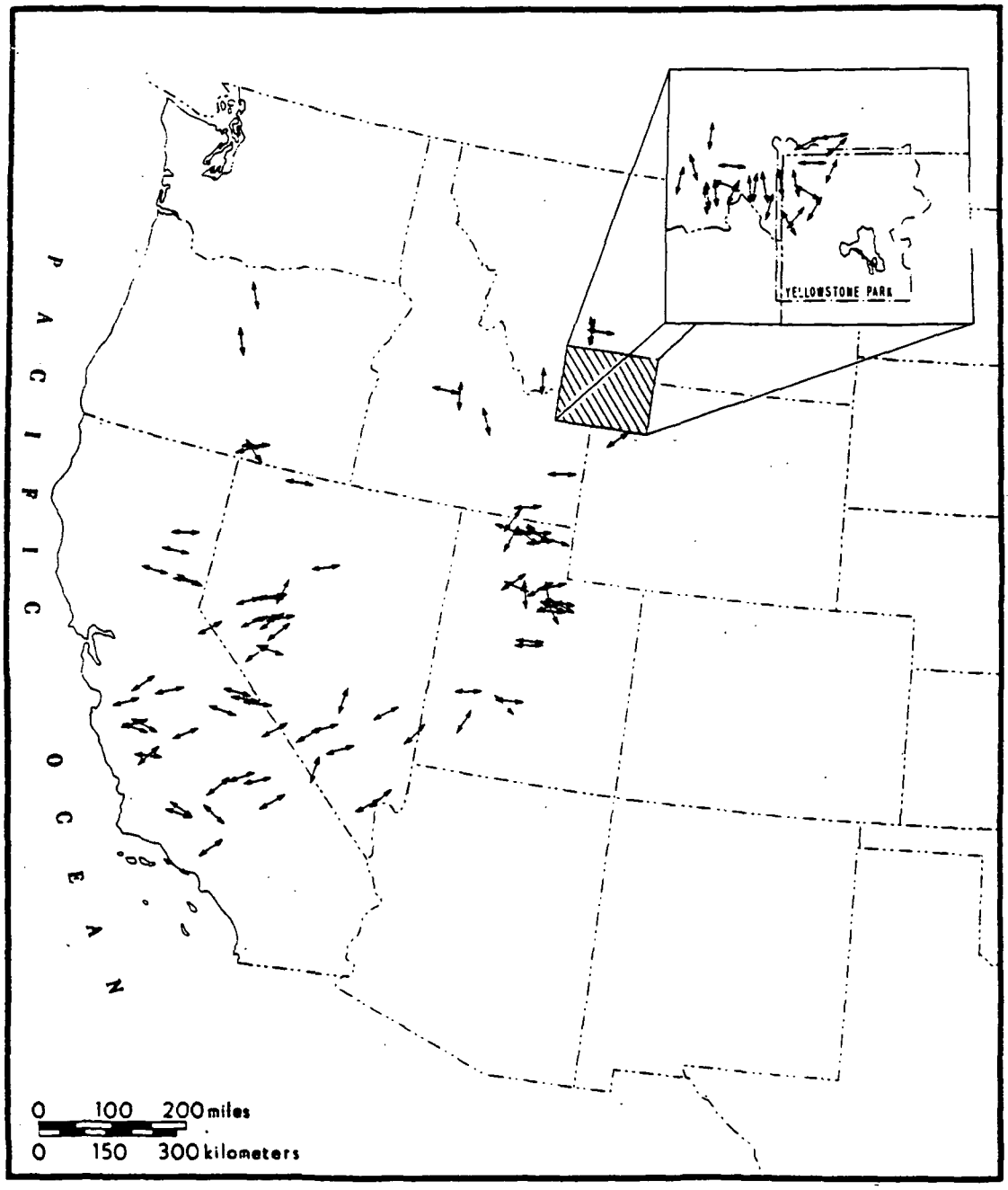

FIG 4 Eddington et al.

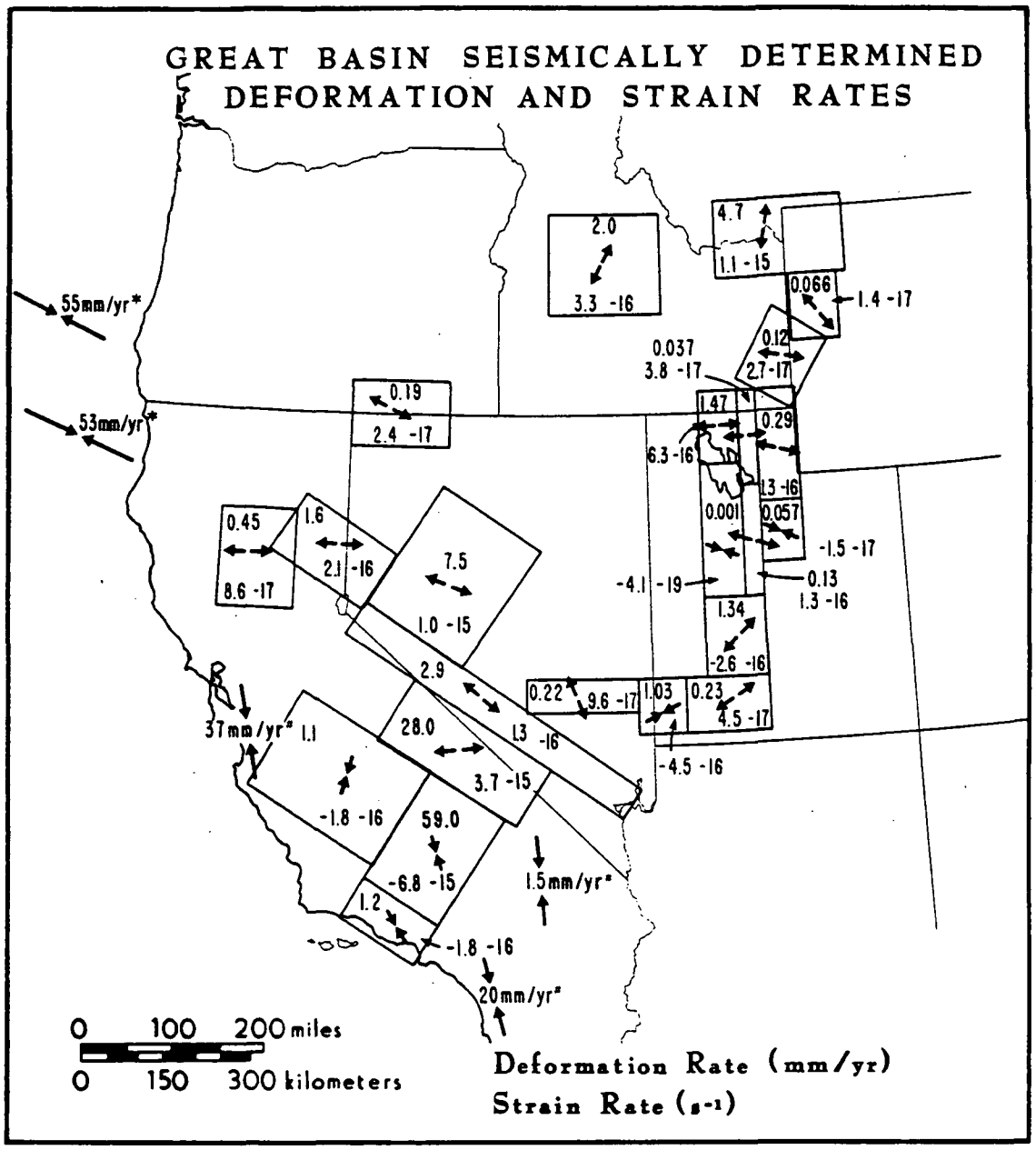

FIG 5 Eddington et al.

ORIGINAL PAGE IS
OF POOR QUALITY

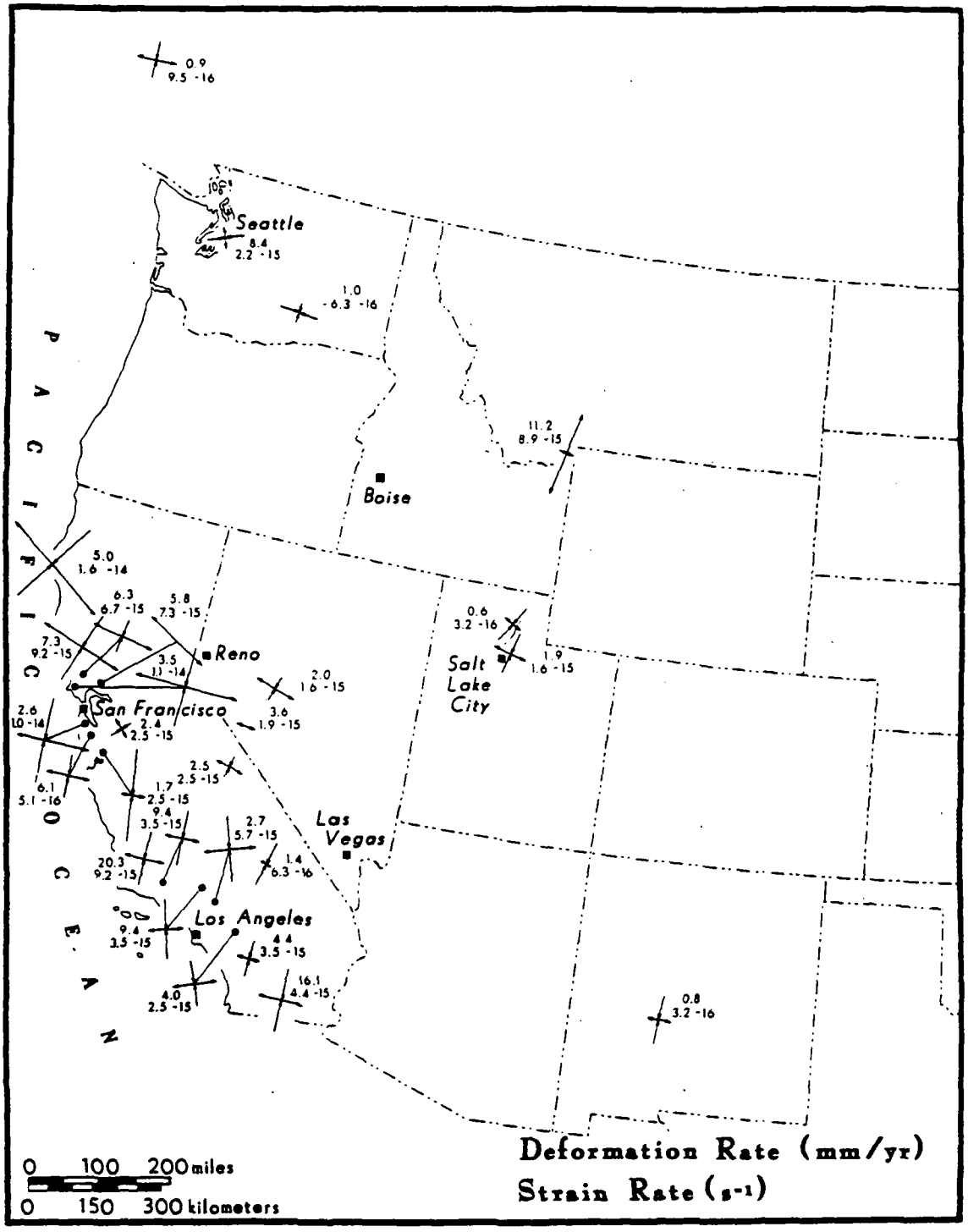

FIG 6 - Eddington et al.

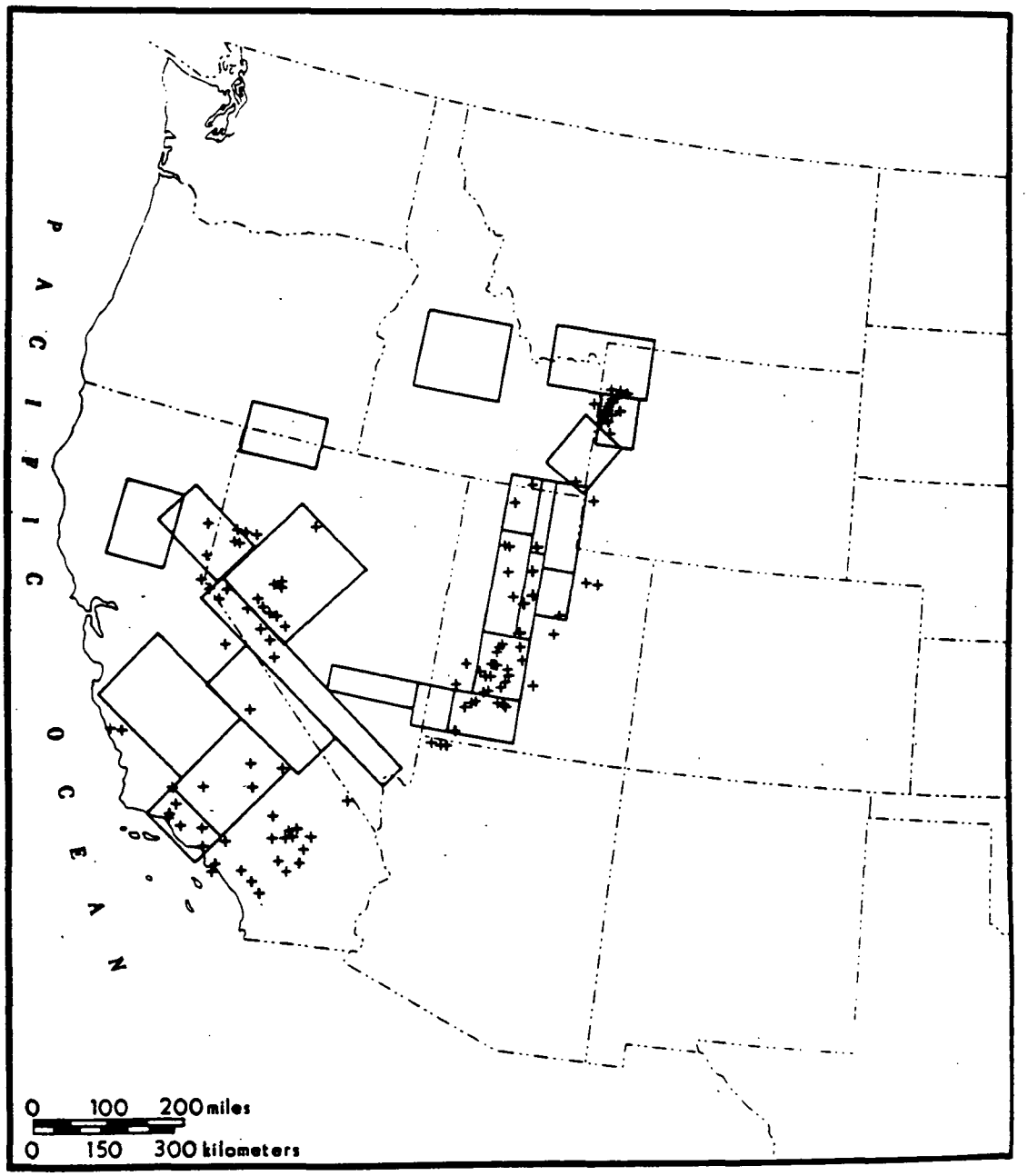

FIG 7 Eddington et al.

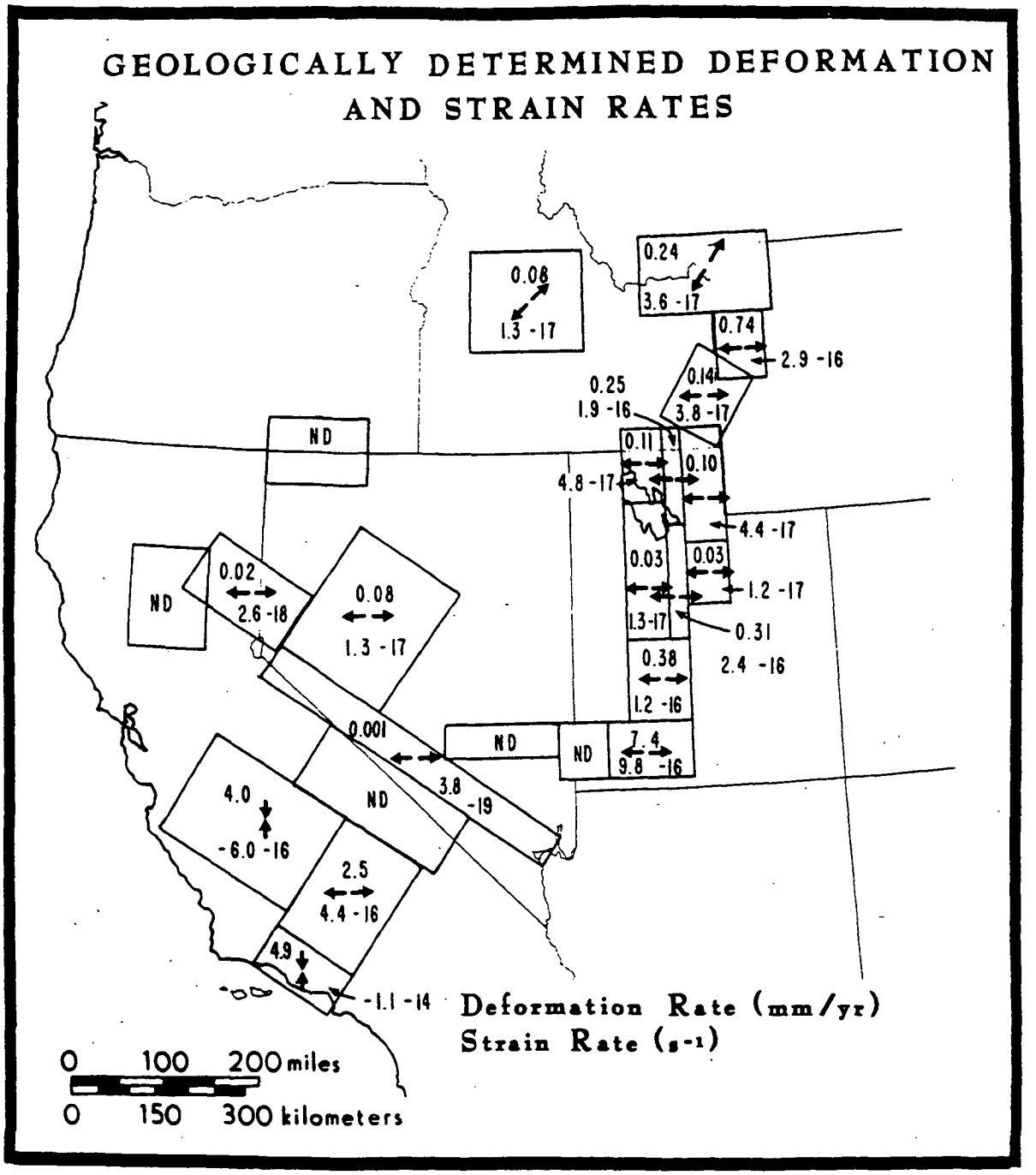

Fig 8 Sbriston et al.

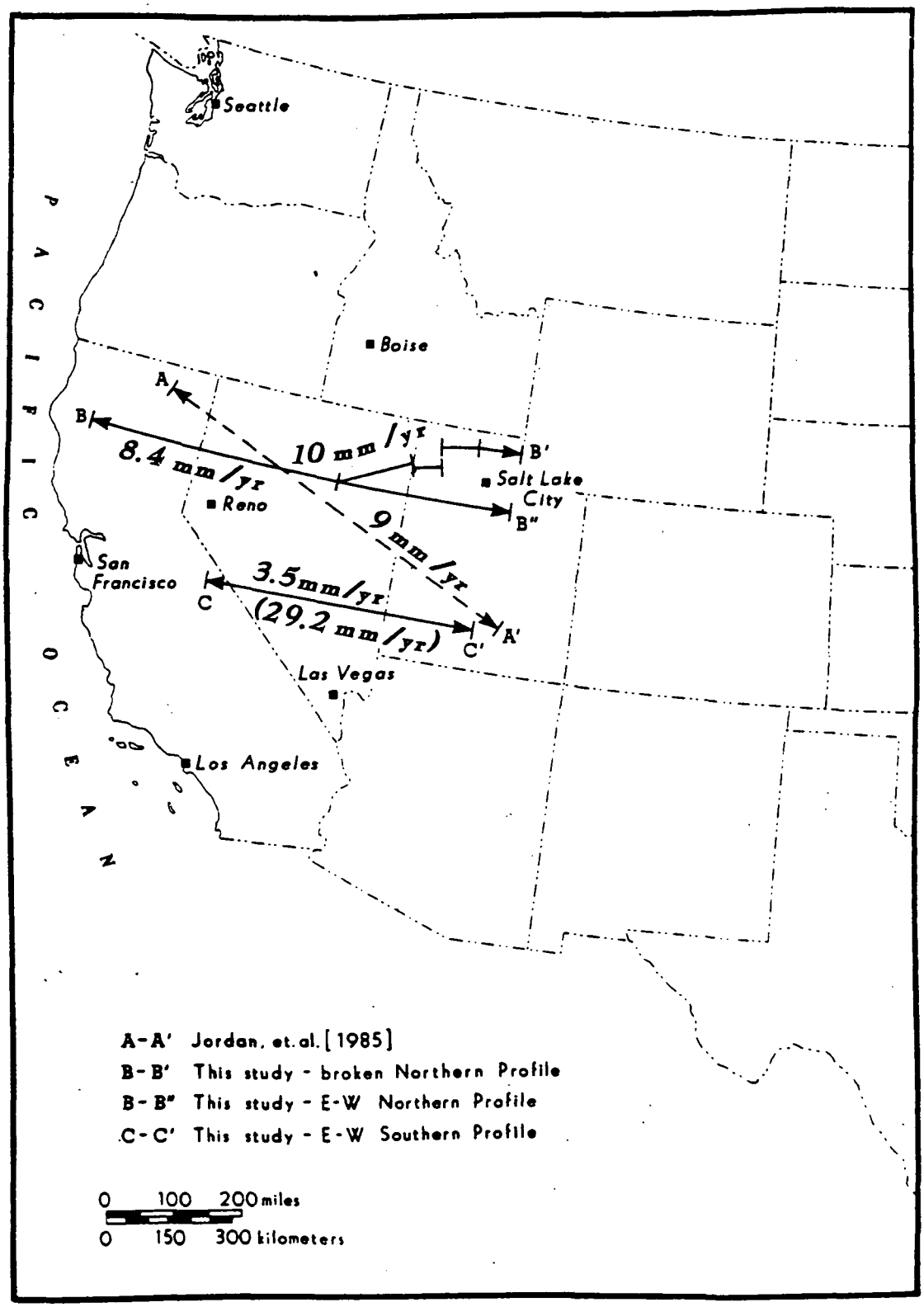

FIG 9 Eddington et al.

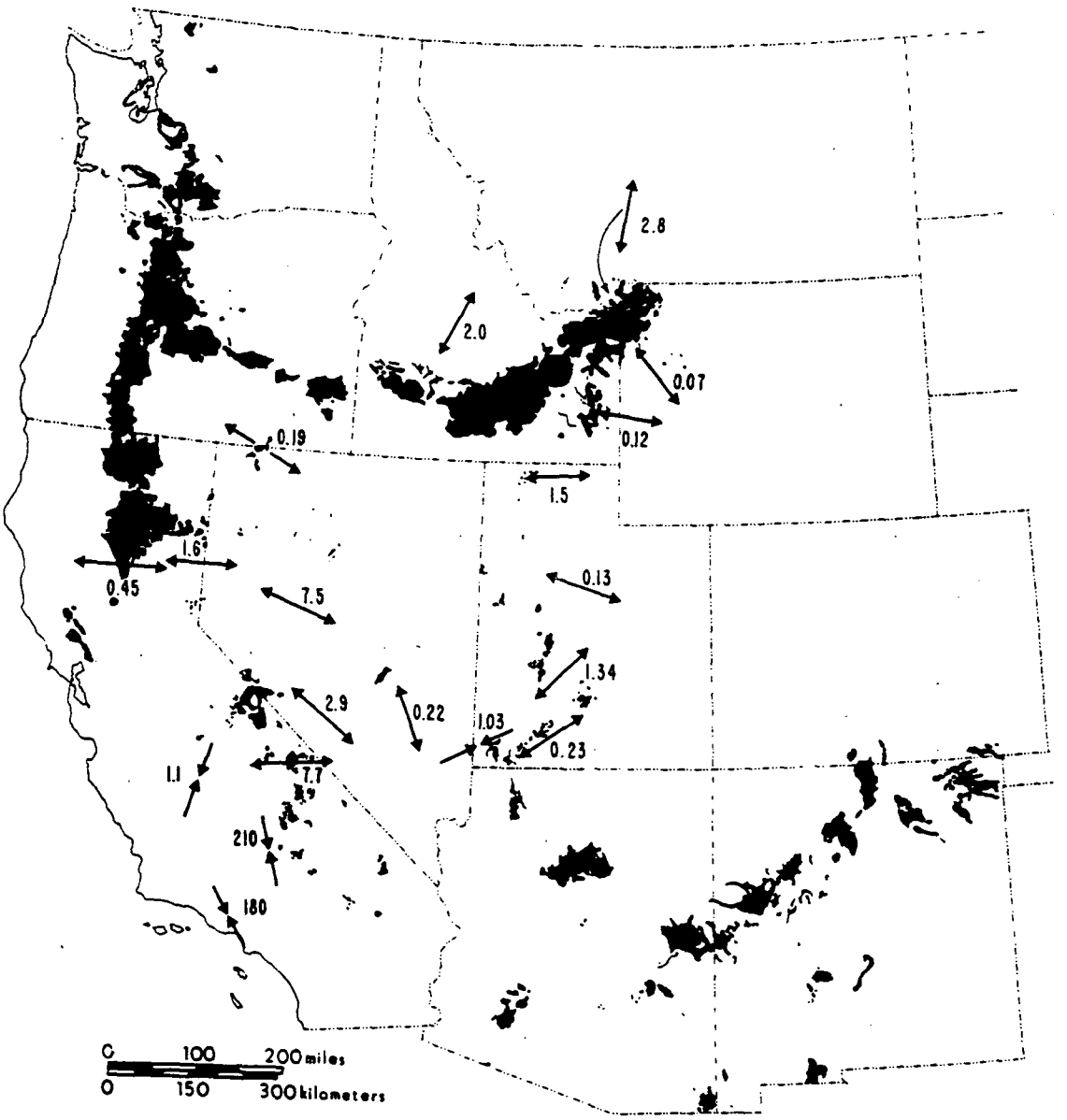

Deformation Rate (mm/yr)

FIG-10 Eddington et al.